Remote Raman Laser Spectroscopy for Investigation of Planetary and Other Celestial Bodies

Natnael Alemayehu Engda

A Thesis Submitted to

The Department of Applied Physics

School of Applied Natural Sciences

Presented in Partial Fulfillment of the Requirement for The Degree of Master's in Applied Physics (Laser Spectroscopy)

Office of Graduate Studies

Adama Science and Technology University

November, 2021
Adama, Ethiopia

Remote Raman Laser Spectroscopy for Investigation of Planetary and Other Celestial Bodies

Natnael Alemayehu Engda

Advisor: Alemu Kebede Hordofa (Ph.D.)

A Thesis Submitted to

The Department of Applied Physics

School of Applied Natural Sciences

Presented in Partial Fulfillment of the Requirement for The Degree of Master's in Applied Physics (Laser Spectroscopy)

Office of Graduate Studies

Adama Science and Technology University

November, 2021
Adama, Ethiopia

Declaration

I hereby declare that this Master thesis entitled "**Remote Raman Laser Spectroscopy for Investigation of Planetary and Other Celestial Bodies**" is my original work. That is, it has not been submitted for the award of any academic degree, diploma or certificate in any other university. All sources of materials that are used for this thesis have been duly acknowledged through citation.

Name: Natnael Alemayehu Engda

Signature: _____

This MSc. thesis has been submitted for examination with my approval as thesis advisor.

Advisor Name: Alemu Kebede Hordofa (Ph.D.)

Signature: _____

Date of submission: _____

Recommendation

I, the advisor of this thesis, hereby certify that I have read the revised version of the thesis entitled "**Remote Raman Laser Spectroscopy for Investigation of Planetary and Other Celestial Bodies**" prepared under my guidance by Natnael Alemayehu Engda submitted in partial fulfillment of the requirements for the degree of Master of Science in Applied Physics (Laser Spectroscopy). Therefore, I recommend the submission of the revised version of the thesis to the department following the applicable procedures.

_____	_____	_____
Name of Advisor	Signature	Date

Approval Page

I, the advisor of the thesis entitled "**Remote Raman Laser Spectroscopy for Investigation of Planetary and Other Celestial Bodies**" and developed by Natnael Alemayehu Engda, hereby certify that the recommendation and suggestions made by the board of examiners are appropriately incorporated into the final version of the thesis.

_____	_____	_____
Advisor	Signature	Date

We, the undersigned, members of the Board of Examiners of the thesis by Natnael Alemayehu Endga have read and evaluated the thesis entitled "Remote Raman Laser Spectroscopy for Investigation of Planetary and Other Celestial Bodies" and examined the candidate during open defense. This is, therefore, to certify that the thesis has been accepted in partial fulfillment of the requirement of the degree of Master of Science in Applied Physics (Laser Spectroscopy).

_____	_____	_____
Chairperson	Signature	Date
_____	_____	_____
Internal Examiner	Signature	Date
_____	_____	_____
External Examiner	Signature	Date

Final approval and acceptance of the thesis is contingent upon submission of its final copy to the Office of Postgraduate Studies (OPGS) through the Department Graduate Council (DGC) and School Graduate Committee (SGC).

_____	_____	_____
Department Head	Signature	Date
_____	_____	_____
School Dean	Signature	Date
_____	_____	_____
Office of Postgraduate Studies (Dean)	Signature	Date

Acknowledgments

First of all, I would like to thank my dearest advisor Dr. Alemu Kebede Hordofa, whom I am very grateful for his keen interest in my work, valuable advice and guidance he provided me in the process of designing and writing up this thesis paper. Since the beginning he supported and appreciated my thesis proposal and guided me throughout the research work.

Secondly, I would like to thank Adama Science and Technology University for awarding me a scholarship opportunity by sponsoring my MSc. study in its Applied Physics Department under School of Applied Natural Sciences which also allowed me to conduct this thesis. With that, I express my heartfelt gratitude to all the staff of the University and more especially of those from Applied Physics Department whom has contributed towards the accomplishment of this research work.

Next, I would love to thank my mother Mrs. Zeritu Demissie Damte and my father Mr. Alemayehu Engda Yematawork for their persistent courage to bring me up and support my work every single day. And I wish to acknowledge all my adored families with my siblings Mr. Dagmawi Alemayehu and Estifanos Alemayehu especially my aunt Ms. Nebiyat Engda Yematawork, they had been there by my side both morally and financially, thank you and bless you all.

Last, but not least, my wholehearted gratitude goes to my best friends Muktar Ahmed Adem and Naod Hailu Dibaba, and my special esteemed revere goes to Hanna Kimemu Biruk. Thank you all for your continuous appreciation and support in the completion of this thesis work.

Dedication

This thesis work is dedicated to my beloved parents and my grandfather Engda Yematawork Aberu.

Table of Contents

List of Tables

List of Figures

List of Acronyms and Abbreviations

ChemCam	Chemistry and Camera
HP	High Pressure
IR	InfraRed
JAXA	Japan Aerospace Exploration Agency
LIBS	Laser Induced Breakdown Spectroscopy
LiDAR	Laser Detection And Ranging
MC	Monoclinic
MSL	Mars Science Laboratory
MUSES-C	Mu Space Engineering Spacecraft C
NASA	National Aerospace and Space Administration
RLS	Raman Laser Spectrometer/Spectroscopy
SAM	Sample Analysis Method
SHERLOC	Scanning Habitable Environments with Raman and Luminescence for Organics and Chemicals
SuperCam	Super Camera
TLS	Tunable Laser Spectrometer
UV	Ultra Violet
XRD	X-Ray Diffraction

Abstract

Raman Laser Spectroscopy is the science based on scattering of Laser light (Raman scattering) to study molecular fingerprints of materials. In Astronomy, this technique has become a key constituent in molecular identification of minerals of celestial bodies in the past few decades. In this research, Raman data of fifteen minerals from Earth analogues and celestial bodies (Asteroids and meteorites) including tridymite, opal, cristoballite, astrophyllite, forsterite, fayalite, glauberite, monticellite, larnite, kirschsteinite, tephroite, dmisteinbergite, lileyite, pyroxene and schorlomite were collected from RRUFF database and analyzed via the software SciDAVis. The result of Raman Spectra of the corresponding fifteen elements were then analyzed and compared with Open Specy website which gives molecular identification instantly. During our investigation, majority of our Raman spectral peaks matched the reference peaks and some in Open Specy with more than 90% accuracy. The result of our finding also well agreed with the results found by other scholars using Raman spectroscopy and other methods including XRD and chemical analysis.

Keywords*: Raman Laser Spectroscopy/Spectrometer, scattering, Raman shift, wavenumber, spectra, mineralogy, meteorite.*

1. Introduction

1.1 Background of the Study

Spectroscopy is one of the most powerful scientific tools for studying nature. The study of celestial bodies using spectroscopy connects astronomy with fundamental physics at atomic and molecular levels. Among numerous spectroscopic techniques, Raman Laser Spectroscopy (RLS) is a promising technique in the field of astrophysics recently (Popescu, 2012).

Raman spectroscopy is based on inelastic scattering of light, and was discovered experimentally in 1928 by C.V. Raman. The Raman technique yields information about vibrational and rotational energy levels of molecules as frequency shifts from the frequency of the exciting light source [$\Delta cm^{-1} = (\upsilon_0 \pm \upsilon_i) - \upsilon_0$], where υ_0 is the absolute frequency of incident light in cm^{-1} and υ_i are vibrational frequencies of the molecule (Angel and Gomer, 2011).

In modern Raman spectroscopy, samples are normally illuminated by a laser at a much higher frequency than that of the vibrational or rotational frequencies of interest. The elastically scattered light is rejected using a combination of extremely narrow band notch filters and proper design of the receiving spectrographs. The remaining (inelastically scattered) light shows diagnostic emission peaks that occur at wavelengths shifted from the exciting laser line by amounts equal to the energy of the excited or relaxed vibrational or rotational states. Thus, using strictly visible light sources and receivers, Raman spectroscopy can yield complementary information about the vibrational transitions observed in infrared emission or reflection spectra (Angel and Gomer, 2011).

In the last few years, Raman spectroscopy has been recognized as a possible method for in-situ planetary and asteroid analysis. Two important fields where Raman spectroscopy is used are mineralogical and organic or biological analysis. It has been shown that Raman spectroscopy can contribute to resolving various questions in the field of planetary and asteroid/meteorite investigations because it allows one to address numerous issues, such as;

1. Analysis of mineralogical and geochemical materials from a planetary surface in order to understand a planet's evolutionary history.

2. Identification of inorganic, organic or biological compounds, which facilitates the search for past or present life on remote celestial bodies (e.g., Mars). This is the main benefit offered by Raman Laser Spectroscopy.

3. Identification of the principal mineral phases (i.e., those making up at least 90% of the material in soils and rocks).

4. Classification of rocks (igneous, sedimentary and metamorphic) and definition of petrogenetic processes.

5. Determination of the oxidation state of planetary elements, e.g., soil, rock surfaces and inside rocks, and the ability to finely differentiate among mineral species.

6. Analysis of the content of volatiles and gaseous inclusions (H_2O, SO_3, CO_2, NO_2, H_2, O_2) in minerals and glasses.

7. Determination of selected minor and trace element contents (e.g., rare earth elements).

8. Determination of reaction kinetics, i.e., oxidation processes on newly exposed surfaces and determination of the reaction products.

9. Morphology of organic inclusions (fossils) and minerals on a micrometer scale obtainable by Raman mapping measurements

10. Identification of water and ice on celestial bodies, e.g., Mars and Churymov/Gerasimenko.

11. Identification of secondary minerals, clays, state of carbonaceous matter and hydrated crystals (Tarcea *et al.,* 2008).

1.2 Statement of the Problem

Astronomical studies in the 21st century have grown and become highly dependent on observations and measurements. Though, they're very challenging (and expensive) despite the seeming growth in the sector especially for developing countries like Ethiopia. Spectroscopic methods are the most utilized ways to study Astronomy but most spectroscopies require sample preparation for analysis which is the main problem in the Astronomical society today because

retrieving samples from celestial bodies is very difficult. Another problem of these spectroscopic methods is that they are studied from Earth in which the atmosphere has a huge impact in the spectrum retrieved from space. Thus, studying remotely is preferable and one of the best ways to do that is through the use of Raman Laser Spectroscopy.

1.3 Objectives of the Study

1.3.1 General objective

The general objective of this thesis is

- To investigate and assess the principles and usages of remote Raman Laser Spectroscopy in Planetary and Asteroid/meteorite investigation.

1.3.2 Specific objectives

- To apply Raman Laser Spectroscopy in the investigation of celestial bodies.
- To analyze Raman spectrum from minerals or meteorite samples using the software SciDAVis.
- To identify elemental or molecular compositions of target samples.

1.4 Significance of the Study

The development of remote Raman Laser Spectroscopy can boost the ability to gather information about the mineralogy and the possible presence of mineral and organic species (their past or present chemical traces) on a planet's and asteroid's/meteorite's surface as well as planetary atmospheres remotely either from ground or space telescopes or even landers. Thus, this study will be so informative to the space science and technology sector of the nation to better understand how to use techniques efficiently and adapt the very modern techniques that the world uses to date.

This new method of engagement will create awareness for the astronomical society on how to adapt such techniques in space exploration. It will serve as the cornerstone for future researchers as it serves as a source of useful information. It will also motivate young researchers to embark

on and participate in the space race of the 21st century with a limited source using this powerful and alternative method of investigating remote celestial bodies.

This study tries to investigate the basic principles of Raman Laser Spectroscopy and its applications on Astrophysics through interpretation of Raman data using the suitable software SciDAVis to show this astrospectroscopic technique is really essential for the development of space exploration.

2. Literature Review

2.1 Raman Scattering and Spectroscopy

There are numerous forms of light-matter interaction: fluorescence and phosphorescence are examples of absorption and subsequent emission of light by matter. Elastic scattering of light, such as Rayleigh scattering by atoms, molecules or phonons, and Mie scattering by dust particles are examples where the wavelength of the light is unchanged. Inelastic scattering such as Compton scattering by charged particles and Raman scattering by molecules or phonons are examples where the wavelength of the light does change (Robin *et al.,* 2019).

Vibrational spectroscopy includes several different techniques, the most important of which are mid-infrared (IR), near-IR, and Raman spectroscopy. Both mid-IR and Raman spectroscopy provide characteristic fundamental vibrations that are employed for the elucidation of molecular structure. Near-IR spectroscopy measures the broad overtone and combination bands of some of the fundamental vibrations (only the higher frequency modes) and is an excellent technique for rapid, accurate quantitation. All three techniques have various advantages and disadvantages with respect to instrumentation, sample handling, and applications (Larkin, 2021).

Vibrational spectroscopy is used to study a very wide range of sample types and can be carried out from a simple identification test to an in-depth, full spectrum, qualitative and quantitative analysis. Samples may be examined either in bulk or in microscopic amounts over a wide range of temperatures and physical states (e.g., gases, liquids, latexes, powders, films, fibers, or as a surface or embedded layer). Vibrational spectroscopy has a very broad range of applications and provides solutions to a host of important and challenging analytical problems (Larkin, 2021).

Raman and mid-IR spectroscopy are complementary techniques and usually both are required to completely measure the vibrational modes of a molecule. Although some vibrations may be active in both Raman and IR, these two forms of spectroscopy arise from different processes and different selection rules. In general, Raman spectroscopy is best at symmetric vibrations of non-polar groups while IR spectroscopy is best at the asymmetric vibrations of polar groups. IR spectroscopy measures transitions between molecular vibrational energy levels as a result of the absorption of mid-IR radiation. This interaction between light and matter is a resonance

condition involving the electric dipole-mediated transition between vibrational energy levels. Raman spectroscopy is a two-photon inelastic light-scattering event. Here, the incident photon is of much greater energy than the vibrational quantum energy, and loses part of its energy to the molecular vibration with the remaining energy scattered as a photon with reduced frequency. In the case of Raman spectroscopy, the interaction between light and matter is an off-resonance condition involving the Raman polarizability of the molecule (Larkin, 2021).

Among scattering effects, Raman scattering is a phenomenon in which photons incident on a sample are inelastically scattered after interacting with vibrating molecules within the sample (Dustin *et al*., 2017). Raman scattering of light by molecules was first predicted using classical quantum theory by Smekal in 1923 and experimentally observed by Raman and Krishnan in 1928 (Robin *et al*., 2019), for which discovery Prof. Raman received the 1930 Nobel Prize in Physics. While Raman spectroscopy is now used in biology and medicine, Raman spectroscopy found its first applications in physics and chemistry and was mainly used to study vibrations and structure of molecules (Dustin *et al.*, 2017).

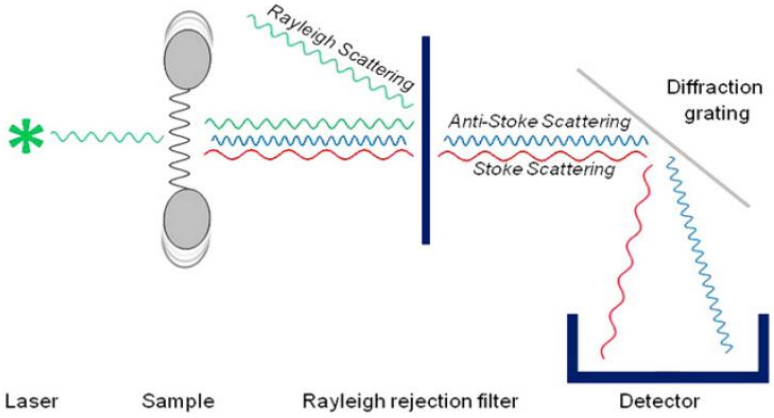

Figure 1: Schematic diagram of a Raman spectrometer (Frezzotti *et al*., 2012).

When light interacts with matter, most of the incident light is scattered elastically (Rayleigh scattering) with no change in energy. Only a small amount, 10^{-8} to 10^{-12}, of the incident radiation is modulated by the molecular scattering system. Depending on the coupling, the incident photons either gain or lose energy. A sample model of scattering system is shown in figure 1 (Tarcea *et al.*, 2008).

In the figure below, a photon with the energy $h\nu_L$ is incident on the scattering system with the energy level $h\nu_R = E_f - E_i$, where i and f label two quantum states. The Stokes– Raman effect results from the transition from the lower energy level E_i to a higher one (E_f). The anti-Stokes effect transfers energy from the system to the incident light wave, which corresponds to the transition from a higher energy level (E_f) to a lower one (E_i). Since the anti-Stokes scattering occurs from a thermally excited state (E_f) which is, according to Boltzmann statistics, less populated than the ground state (E_i), the anti-Stokes is less than the Stokes intensity (Tarcea *et al.*, 2008).

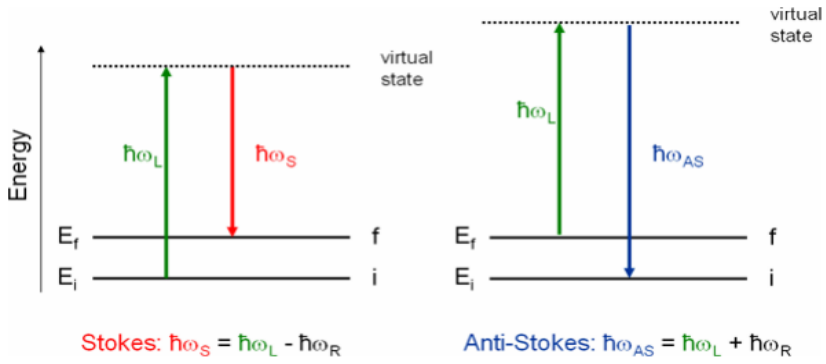

Figure 2: Raman scattering process (Tarcea *et al.*, 2008).

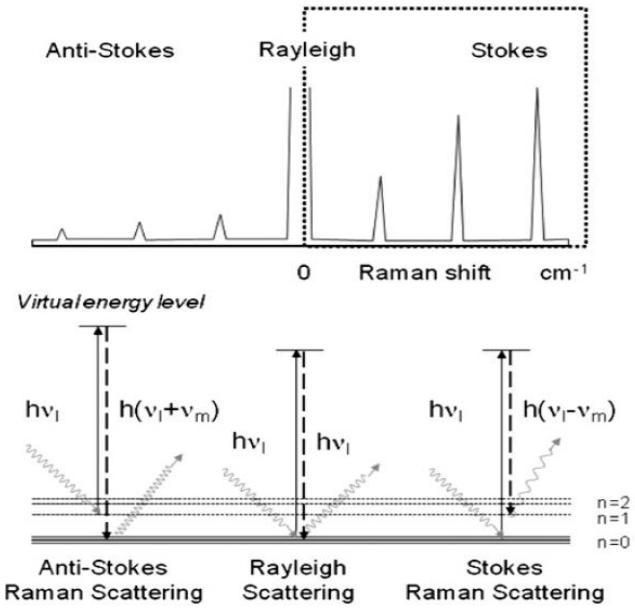

Figure 3: Energy level scheme for elastic (Rayleigh) and inelastic (Raman) scattering at the frequency of the light source (ν_l), and Raman and Rayleigh spectra. The molecular vibration of the analyzed sample is of frequency ν_m (Frezzotti *et al*., 2012).

The mathematical aspects of Raman spectra are discussed as follows. First of all, we need to know how intensity and wavenumber or Raman shift can be calculated. The intensity of Raman scattered light from a sample, $I(\nu)_R$, is given by Eq. 1:

$$I(\nu)_R = \frac{16\pi^3}{45 \cdot 3^2 \cdot c^4} \times \frac{h I_L N (\nu_0 - \nu)^4}{\mu\nu(1 - e^{-h\nu/kT})} \times [45\,(\alpha'_a)^2 + 7\,(\gamma'_a)^2] \quad (1)$$

where c = speed of light, h = Planck's constant, I_L = Excitation intensity, N = Number of scattering molecules, ν = Molecular vibrational frequency in Hertz, ν_0 = Laser excitation frequency in Hertz, μ = Reduced mass of the vibrating atoms, k = Boltzmann constant, T = Absolute temperature, α'_a = Mean value invariant of the polarizability tensor and γ'_a = Anisotropy invariant of the polarizability tensor (Pelletier, 2003).

The important parameters here are the wavelength (λ, length of 1 wave), frequency (ν, number cycles per unit time), and wavenumbers ($\tilde{\nu}$, number of waves per unit length) and are related to one another by the following expression:

$$\tilde{\nu} = \frac{\nu}{c/n} = 1 / \lambda, \quad (2)$$

where c is the speed of light and n the refractive index of the medium it is passing through. In quantum theory, radiation is emitted from a source in discrete units called photons where the photon frequency, ν, and photon energy, E_p, are related by:

$$E_p = h\nu, \quad (3)$$

where h is Planck's constant. Photons of specific energy may be absorbed (or emitted) by a molecule resulting in a transfer of energy. In absorption spectroscopy, this will result in raising the energy of molecule from ground to a specific excited state (Larkin, 2011).

Typically the rotational (E_{rot}), vibrational (E_{vib}), or electronic (E_{el}) energy of molecule is changed by ΔE:

$$\Delta E = E_p = h\nu = hc\tilde{\nu}, \quad (4)$$

and in the absorption of a photon the energy of the molecule increases and ΔE is positive. To a first approximation, the rotational, vibrational, and electronic energies are additive: (Larkin, 2011)

$$E_T = E_{el} + E_{vib} + E_{rot}. \quad (5)$$

We are concerned with photons of such energy that we consider E_{vib} alone and only for condensed phase measurements. Higher energy light results in electronic transitions (E_{el}) and lower energy light results in rotational transitions (E_{rot}). However, in the gas-state both IR and Raman measurements will include $E_{vib} + E_{rot}$ (Larkin, 2011).

Raman spectra are usually plotted in terms of the wavenumber shift from the incident excitation radiation. This shift is defined as follows:

$$\Delta\tilde{\nu} = \tilde{\nu}_p - \tilde{\nu}_{scat}, \quad (6)$$

where $\tilde{\nu}_p$ is the wavenumber of the pump beam with angular frequency ω_p and $\tilde{\nu}_{scat}$ is the wavenumber of the scattered light accordingly. For Stokes Raman scattering, $\tilde{\nu}_{scat} = \tilde{\nu}_p - \tilde{\nu}_{osc}$ (where $\tilde{\nu}_{osc}$ is the molecule or lattice vibration wavenumber) and $\Delta\tilde{\nu}$ is positive. By contrast, for anti-Stokes Raman scattering, $\tilde{\nu}_{scat} = \tilde{\nu}_p + \tilde{\nu}_{osc}$ and $\Delta\tilde{\nu}$ is negative (Robin *et al*. 2019).

Thus, $\tilde{\nu}_{scat} = \tilde{\nu}_p \pm \tilde{\nu}_{osc}$ (7)

and the frequency shift in molecular or lattice vibration is what we will be looking for in order to find the scattered frequency shift which is the Raman shift we will get to have our Raman spectrum (Robin *et al*. 2019).

Traditionally, energies of molecular vibrational modes are expressed with units of wavenumbers, or cm^{-1}. This convention is a result of the origins of Raman spectroscopy in chemistry and the

similarity of the technique to IR absorption spectroscopy, which also probes molecular vibrations (Dustin *et al*., 2017).

Some of the **advantages** of Raman spectroscopy are:

1. Sample Preparation; little to no sample preparation is required is most cases. The sample can be placed into the holder position and a spectrum can be retrieved.

2. Water as a solvent; water is a weak scatterer, thus, it can be used as a solvent for a 'difficult sample' - no special accessories are required for measuring in aqueous solutions.

3. No need for nitrogen purging of the optical bench; water and carbon dioxide vapors are very weak scattering species.

4. Cheap and sample holders; inexpensive glass sample holders are ideal in most cases.

5. Cleaner Spectra; Raman spectra are "cleaner" than mid-IR spectra - Raman bands are narrower, and overtone and combination bands are generally weak.

6. Wide range of molecules to investigate; the standard spectral range reaches well below 400 cm^{-1}, making the technique ideal for both organic and inorganic species.

7. Investigate weak IR bands; Raman spectroscopy can be used to measure bands of symmetric linkages which are weak in an infrared spectrum such as C=C, C-S and S-S (Adamo, 2021).

Disadvantages of Raman Spectroscopy are:

1. Due to the low Raman intensities the detector sensitivity is paramount.

2. Instrumentation is more expensive than typical mid-range IR.

3. Laser can destroy sections of the sample if the power setting is too high.

4. Fluorescence caused by the laser is a major concern with some samples (Adamo, 2021).

In Raman spectroscopy, scattered light is detected by a spectrometer to identify the "chemical fingerprint" of the test sample. By using spectral data, a material can be recognized or classified.

The results of a Raman spectroscopy analysis are usually represented graphically, with the intensity of the scattered light (y-axis) plotted against the frequency of light (x-axis). Also considered an indication of energy, frequency is usually measured by a unit known as the wavenumber, which is represented as reciprocal centimeters (cm^{-1}). Frequencies are plotted in relation to that of the laser, since the change in energy of the light is of interest (Smith, 2019).

The identification of a mineral by Raman spectroscopy is a comparative method. Only in some rare cases is it possible to calculate and predict the peak positions of a given substance. Therefore the necessity of a collection or data base of reference spectra is extremely important (Hänni *et al*., 1997).

The common practice to plotting Raman spectra is intensity, or "Count Rate", on the y-axis and the frequency of the "Raman Shift" along the x-axis. Raman shift is the difference in frequency between the laser light and the scattered light. This difference is unrelated to laser's wavelength and expressed as wavenumbers. Count Rate is the quantity of events the spectrometer detects for the particular Raman shift per second and is relative to the strength of light detected (Smith, 2019).

You can tell a great deal about a material from its Raman spectrum, with different features relating to different aspects of the material. One way is to observe the Raman shifts and relative intensities of all of the Raman bands of the material**.** With this, we can identify the material (Wilcock, 2021) by recognizing molecular functional groups, which are distinct subunits of a molecule. The vibrations of functional groups appear in Raman spectra at distinctive Raman shifts. These characteristic shifts allow for an unknown compound to be linked to a known class of substances (Smith, 2019).

A second way is to observe individual band changes. Here, a band may shift, narrow or broaden, or vary in intensity. These changes can reveal information about stresses in the sample, variations in crystallinity, and the amount of material respectively. Third, is to observe variations in spectra with position on the sample. This will reveal changes in the uniformity (homogeneity) of the material. You can analyze at several arbitrary points, or systematically measure an array of points (enabling the production of images of composition, stress, crystallinity, etc.) (Wilcock, 2021).

A fourth approach involves the use of interpretation software that has a spectral database and a comparison algorithm. This software generates a matching factor that can range from 0 (“no match”) to 100 ("perfect match”). User typically defines a threshold for deeming a test sample a suitable match to a known substance (Smith, 2019).

2.2 Mineralogy Theories

Silica is one of the constituent minerals in the Earth’s crustal rocks, and is one of the minor minerals that is often distributed in extraterrestrial materials such as lunar and Martian meteorites, returned samples (Apollo and Luna collections), and the parent bodies (e.g., the Moon and Mars). Over the past ten years, various types of silica polymorphs (e.g., quartz, tridymite, cristobalite, moganite, coesite, stishovite, seifertite, and baddeleyite-type SiO_2) and non-crystalline silica (high-pressure (HP) silica glass and opal) have been reported in lunar and Martian rocks using microanalyses and studying the celestial bodies through remote-sensing observations, although a lack of the diversity and wide distribution was believed before. For example, several previous investigations have supported the hypothesis that few high-pressure phases are included in lunar meteorites, despite the existence of many craters and regoliths, because a part of them (e.g., the high-pressure SiO_2 phases) may be volatilized during impact collisions under the high vacuum condition of the Moon. However, recent studies have revealed that coesite, stishovite, and seifertite lie in several lunar meteorites and an Apollo collection (Kayama *et al*., 2018).

Hydrothermal silica was believed to be absent from extraterrestrial materials, but moganite and opal-A, originating from the fluid activity of the parent bodies, have recently been discovered from lunar and Martian meteorites. Opaline silica deposits have also been observed in association with Martian volcanic materials by the Mars rover “Spirit and Opportunity”. In addition, silica nanoparticles were detected in Enceladus by the Cassini spacecraft. Of course, for decades, many researchers have reported igneous silica such as quartz, tridymite, and cristoballite in various types of extraterrestrial materials, especially in lunar samples (lunar meteorites and Apollo and Luna collections) and Martian meteorites. From the latest viewpoint of planetary science, there seems to be a wide variety of silica polymorphs in the solar system (Kayama *et al*., 2018).

The study of minerals on Earth is a bulky concept so we discuss them within groups such as the common group olivine and pyroxenes (single-chain silicates). Among numerous species that are of extraterrestrial origin, olivine includes forsterite, fayalite, glauberite, larnite, monticellite, kirschsteinite and tephorite and pyroxene includes dmisteinbergite, lileyite, pyroxene, and schorlomite (Hoefen, *et al*., 2003).

The Raman spectra of humite minerals are of importance as these minerals are likely to be found in meteorites. Raman spectra of olivines have been studied. The humite structure may be treated as olivine silicate layers interspersed with brucite layers. Olivines have compositions M_2^{2+} SiO_4 where M^{2+} is Mg, Ca, Mn, Fe, Co and Ni (Frost *et al.,* 2007).

Mg-rich olivine has also been discovered in meteorites, on the Moon and Mars, falling into infant stars, as well as on asteroid 25143 Itokawa. Such meteorites include chondrites, collections of debris from the early Solar System and pallasites, mixes of iron-nickel and olivine (Hoefen, *et al*., 2003).

The spectral signature of olivine has been seen in the dust disks around young stars. The tails of comets (which formed from the dust disk around the young Sun) often have the spectral signature of olivine, and the presence of olivine was verified in samples of a comet from the Stardust spacecraft in 2006. Comet-like (magnesium-rich) olivine has also been detected in the planetesimal belt around the star Beta Pictoris (Greaves *et al*., 2012).

Discovery of some pyroxenes have also caught our interest in mineralogy of the solar system. They were detected in many stone and some stony-iron meteorites, rocks and regolith of the Moon and Mars (Huang *et al*., 2000).

2.3 Current Developments of Remote RLS in Astronomy

Raman Laser Spectrometer (RLS) provides geological and mineralogical information on igneous, metamorphic, and sedimentary processes, especially regarding water-related interactions (chemical weathering, chemical precipitation from brines, etc.). In addition, it also permits the detection of a wide variety of organic functional groups. Raman can contribute to the

tactical aspects of exploration by providing a quick assessment of organic content (Jorge *et al*., 2017).

To date, there have been a few space missions for asteroid/comet and planetary investigations and most of them use direct sample analysis using traditional spectroscopic techniques. However, in recent years, the need to use laser spectroscopy, especially Raman spectroscopy, is growing rapidly since it is very precise and non-destructive method with minimal sample preparation making it optimum for remote investigation of astromaterial (Agle *et al.*, 2014).

The Hayabusa mission was a robotic spacecraft developed by the Japan Aerospace Exploration Agency (JAXA) to return a sample of material from a small near-Earth asteroid named 25143 Itokawa to Earth for further analysis. Hayabusa, formerly known as MUSES-C for Mu Space Engineering Spacecraft C, was launched on 9 May 2003 and rendezvoused with Itokawa in mid-September 2005. After arriving at Itokawa, Hayabusa studied the asteroid's shape, spin, topography, color, composition, density, and history. In November 2005, it landed on the asteroid and collected samples in the form of tiny grains of asteroidal material, which were returned to Earth aboard the spacecraft on 13 June 2010. Among its instruments, it used LiDAR technology, purely a laser application, which was used to calculate distance of the spacecraft from the asteroid precisely and took relatively clear images of the asteroid (Yoshimitsu *et al.*, 2010).

Rosetta was a space probe built by the European Space Agency launched on 2 March 2004. Along with Philae, its lander module, Rosetta performed a detailed study of comet 67P/Churyumov–Gerasimenko (67P). The lander used four diode lasers for spectroscopic analysis of the comet's surface samples (Agle *et al.*, 2014).

In January 2004, two robotic geologists named Spirit and Opportunity landed on opposite sides of the red planet. With far greater mobility than the 1997 Mars Pathfinder rover, these robotic explorers have trekked for miles across the Martian surface, conducting field geology and making atmospheric observations. Carrying identical, sophisticated sets of science instruments, both rovers have found evidence of ancient Martian environments where intermittently wet and habitable conditions existed. With data from the rovers, mission scientists have reconstructed an ancient past when Mars was awash in water. Spirit and Opportunity each found evidence for past

wet conditions that possibly could have supported microbial life. Opportunity's study of "Eagle" and "Endurance" craters revealed evidence for past inter-dune playa lakes that evaporated to form sulfate-rich sands. The sands were reworked by water and wind, solidified into rock, and soaked by groundwater. These sample analysis were performed using traditional spectroscopic methods (Nelson, 2014).

Curiosity is a car-sized Mars rover designed to explore the Gale crater on Mars as part of NASA's Mars Science Laboratory (MSL) mission for an investigation of the Martian climate and geology, assessment of whether the selected field site inside Gale has ever offered environmental conditions favorable for microbial life (including investigation of the role of water), and planetary habitability studies in preparation for human exploration. It involved two laser applications among its advanced technologies. They are ChemCam and SAM instruments that involve LIBS and a tunable laser spectrometer (TLS), respectively (Amos, 2012).

Perseverance, nicknamed Percy, is a car-sized Mars rover designed to explore the Jezero crater on Mars as part of NASA's Mars 2020 mission. It was manufactured by the Jet Propulsion Laboratory and was launched on 30 July 2020 and landed on Mars on 18 February 2021 (Taylor, 2020).

Among its highly advanced instruments, two include laser spectroscopic techniques. One is SuperCam which is essentially a next-generation version of the Curiosity rover's ChemCam. Like its predecessor, SuperCam can use an infrared laser beam to heat the material it impacts to around 18,000 degrees Fahrenheit (10,000 degrees Celsius) — a method called laser induced breakdown spectroscopy, or LIBS — and vaporizes it. A special camera can then determine the chemical makeup of these rocks from the plasma that is created. The other is Scanning Habitable Environments with Raman and Luminescence for Organics and Chemicals (SHERLOC), an ultraviolet Raman spectrometer that uses fine-scale imaging and an ultraviolet (UV) laser to determine fine-scale mineralogy and detect organic compounds (Beegle, *et al.,* 2014).

3. Methods of the Study

3.1 Data Collection Method

Raman spectra of minerals of astronomical analogues on Earth were collected primarily from RRUFF database. Here, one can find Raman and XRD data of numerous minerals including that of meteorites and their respective synthetic data. Some target minerals that may be found beyond Earth, that is, those that can be of any unearthly origin were selected. These minerals targeted involved tridymite, opal, cristoballite, astrophyllite, olivines such as forsterite, fayalite, glauberite, larnite, monticellite, kirschsteinite and tephroite and pyroxenes such as dmisteinbergite, lileyite, pyroxene, and schorlomite. Thus, intensity vs. wavenumber (Raman shift) data of these targets was obtained from this website of database.

Screenshots of some of these data were taken placed as a sample in appendix.

3.1.1 Tridymite (SiO_2)

1. Tridymite (RRUFFID = R090042)

- Locality: The Fukang Pallasite meteorite, Gobi Desert, China, found in 2001.
- Source: Dante Lauretta.
- Description: Colorless micro-crystal, as an inclusion in olivine. Masami Kanzaki (Okayama University) suggests this is polytype tridymite MC.
- Status: The identification of this mineral has been confirmed by single-crystal X-ray diffraction.

2. Tridymite (RRUFFID = R090063)

- Locality: Mount Howe 88403 meteorite, likely formed during impact on a chondritic-parent body.
- Source: Devin L. Schrader and Dante S. Lauretta.
- Description: Imbedded in a polished slab, associated with kamacite, taenite, troilite, and schreibersite. Masami Kanzaki (Okayama University) suggests this is polytype tridymite MC.

- Status: The identification of this mineral has been determined only by Raman Spectroscopy.

3. Tridymite (RRUFFID = R040143)

- Locality: Big Lue Mountain, Highway 78, Greenlee County, Arizona, USA.
- Source: University of Arizona Mineral Museum.
- Description: Colorless thin hexagonal plates. Masami Kanzaki (Okayama University) suggests this is polytype tridymite PO-10.
- Status: The identification of this mineral is confirmed by single-crystal X-ray diffraction and chemical analysis.

4. Tridymite (RRUFFID = R160073)

- Locality: Synthetic.
- Source: Unkown.
- Description: Fine white powder.
- Status: The identification of this mineral is not yet confirmed.

3.1.2 Opal ($SiO_2 \cdot nH_2O$)

1. Opal (RRUFFID = R060652)

- Locality: Ethiopia.
- Source: Gemological Institute of America.
- Description: Colorless cloudy glassy fragment, variety opal-C.
- Status: The identification of this mineral has been confirmed by X-ray diffraction and chemical analysis.

2. Opal (RRUFFID = X080017)

- Locality: Synthetic.
- Source: Gemological Institute of America.
- Description: Polished Gilson cabachon, 1.58 ct.

- Status: The identification of this mineral has been determined only by Raman spectroscopy.

3.1.3 Cristoballite (SiO_2)

1. Cristoballite (RRUFFID = R061064)

- Locality: Ellora Caves, India.
- Source: Harvard Mineralogical Museum.
- Description: Colorless single crystals, octahedra and groups of octahedra, some have transformed to quartz. Sample used in Downs and Palmer (1994).
- Status: The identification of this mineral is confirmed by single-crystal X-ray diffraction and chemical analysis.

2. Cristoballite (RRUFFID = X050047)

- Locality: Mayen, Eifel, Germany.
- Source: CIT.
- Description: None.
- Status: The identification of this mineral has been determined only by Raman spectroscopy.

3.1.4 Astrophyllite ($K_2NaFe_7^{2+}Ti_2(Si_4O_{12})_2O_2(OH)_4F$)

1. Astrophyllite (RRUFFID = R060103)

- Locality: Brivik, Norway.
- Source: University of Arizona Mineral Museum.
- Description: Brown fragment embedded in matrix.
- Status: The identification of this mineral is confirmed by single-crystal X-ray diffraction and chemical analysis.

2. Astrophyllite (RRUFFID = R060202)

- Locality: Demix Quarry, Mont Saint-Hilaire, Rouville County, Quebec, Canada.

- Source: Royal Ontario Museum.
- Description: Aggregate of brown splintered wafers.
- Status: The identification of this mineral is confirmed by X-ray diffraction and chemical analysis.

3.1.5 Forsterite ($Mg_2(SiO_4)$)

1. Forsterite (RRUFFID = X050081)

- Locality: East Africa.
- Source: G.R. Rossman.
- Description: None.
- Status: The identification of this mineral has been determined only by Raman spectroscopy.

2. Forsterite (RRUFFID = R100099)

- Locality: Synthetic.
- Source: American Museum of Natural History.
- Description: Colorless fragments.
- Status: The identification of this mineral is confirmed by single-crystal X-ray diffraction and chemical analysis.

3.1.6 Fayalite ($Fe_2(SiO_4)$)

1. Fayalite (RRUFFID = X050077)

- Locality: Synthetic.
- Source: G.R. Rossman.
- Description: None.
- Status: The identification of this mineral has been determined only by Raman spectroscopy.

2. Fayalite (RRUFFID = R070157)

- Locality: Coso Hot Springs, Inyo County, California, USA.
- Source: James Shigley.
- Description: Brown transparent tabular crystals associated with fine grained quartz.
- Status: The identification of this mineral is confirmed by single-crystal X-ray diffraction and chemical analysis.

3. Fayalite (RRUFFID = R100103)

- Locality: Franklin, Sussex County, New Jersey, USA.
- Source: American Museum of Natural History.
- Description: Dark brown fragment.
- Status: The identification of this mineral is confirmed by single-crystal X-ray diffraction and chemical analysis.

3.1.7 Glauberite ($Na_2Ca(SO_4)_2$)

1. Glauberite (RRUFFID = R050350)

- Locality: Soda Lake, San Luis Obispo County, California, USA.
- Source: California Institute of Technology.
- Description: Colorless tabular crystal.
- Status: The identification of this mineral is confirmed by X-ray diffraction and chemical analysis.

2. Glauberite (RRUFFID = R070322)

- Locality: Salton Sea, Imperial County, California, USA.
- Source: James Shigley.
- Description: Colorless tabular crystal.
- Status: The identification of this mineral is confirmed by X-ray diffraction.

3.1.8 Larnite ($Ca_2(SiO_4)$)

Larnite (RRUFFID = R070530)

- Locality: Larne, County Antrim, Northern Ireland, UK.
- Source: Michael Scott.
- Description: Light gray massive.
- Status: The identification of this mineral has been confirmed by single-crystal X-ray diffraction.

3.1.9 Monticellite ($CaMg(SiO_4)$)

1. Monticellite (RRUFFID = R040115)

- Locality: Magnet Cove, Arkansas, USA.
- Source: University of Arizona Mineral Museum.
- Description: Brown blebs in matrix.
- Status: The identification of this mineral has been confirmed by X-ray diffraction and chemical analysis.

2. Monticellite (RRUFFID = R100108)

- Locality: Oka, Deux-montagnes County, Quebec, Canada.
- Source: American Museum of Natural History.
- Description: Pale brown transparent fragment.
- Status: The identification of this mineral has been confirmed by X-ray diffraction and chemical analysis.

3.1.10 Kirschsteinite ($CaFe^{2+}(SiO_4)$)

Kirschsteinite (RRUFFID = R070266)

- Locality: Dolores mine, Pastrana, Mazarrón, Murcia, Spain.
- Source: Michael Scott.
- Description: Aggregate of vitreous brown rhombic prismatic crystals with conchoidal fracture.
- Status: The identification of this mineral has been confirmed by X-ray diffraction and chemical analysis.

3.1.11 Tephroite ($Mn_2^{2+}(SiO_4)$)

1. Tephroite (RRUFFID = R060141)

- Locality: Franklin, New Jersey, USA.
- Source: Marcus Origlieri.
- Description: Tan colored massive, associated with reddish zincite and metallic franklinite.
- Status: The identification of this mineral has been confirmed by X-ray diffraction and chemical analysis.

2. Tephroite (RRUFFID = R070511)

- Locality: Langban, Filipstad, Varmland, Sweden.
- Source: Michael Scott.
- Description: Light gray vitreous massive.
- Status: The identification of this mineral is confirmed by single-crystal X-ray diffraction and chemical analysis.

3.1.12 Dmisteinbergite ($Ca(Al_2Si_2O_3)$)

1. Dmisteinbergite (RRUFFID = R130085)

- Locality: CV3 type carbonaceous chondrite NWA 2086 at University of Szeged, Hungary.
- Source: Krisztian Fintor.
- Description: Refractory mineral among clinopyroxene-grossular and spinel-gehlenite assemblage.
- Status: The identification of this mineral is confirmed by electron backscatter diffraction and chemical analysis.

2. Dmisteinbergite (RRUFFID = R130087)

- Locality: Katashina Village, Gunma Prefecture, Japan.
- Source: Michael Scott.

- Description: Colorless platelets with pearly luster.
- Status: The identification of this mineral is not yet confirmed.

3.1.13 Lileyite ($Ba_2Ti_2Na_2Fe^{2+}Mg(Si_2O_7)_2O_2F_2$)

Lileyite (RRUFFID = R140773)

- Locality: Graulay, Hillesheim, Eifel, Rhineland-Palatinate, Germany.
- Source: Ch. and H. Schäfer.
- Description: Reddish brown prismatic crystals with fine striations, associated with pyroxene, schorlomite and leucite.
- Status: The identification of this mineral has been confirmed by single-crystal X-ray diffraction.

3.1.14 Pyroxene (R110130)

- Locality: Little Deer Creek eclogite, Skagit County, Washington, USA.
- Source: Bart Cannon.
- Description: Blocky transparent green crystals coating a surface of a rock. Single crystal X-ray diffraction shows that this sample is composed of exsolution lamellae of diopside and jadeite.
- Status: The identification of this mineral has been confirmed only by single-crystal X-ray diffraction.

3.1.15 Schorlomite ($Ca_3Ti_2(SiFe_2^{3+})O_{12}$)

1. Schorlomite (RRUFFID = R060125)

- Locality: Magnet Cove, Arkansas, USA.
- Source: University of Arizona Mineral Museum.
- Description: Black massive.
- Status: The identification of this mineral has been confirmed by X-ray diffraction and chemical analysis.

2. Schorlomite (RRUFFID = R060349)

- Locality: Sundsvall, Medelpad, Sweden.
- Source: Marcus Origlieri.
- Description: Black massive, intimately associated with andradite.
- Status: The identification of this mineral has been confirmed by single-crystal X-ray diffraction and chemical analysis.

3. Schorlomite (RRUFFID = R140772)

- Locality: Graulay, Hillesheim, Eifel, Rhineland-Palatinate, Germany.
- Source: Ch. and H. Schäfer.
- Description: Associated with noonkanbahnite, pyroxene and oxyphlogopite.
- Status: The identification of this mineral has been confirmed only by single crystal X-ray diffraction.

3.2 Data Analysis Methods

3.2.1 Software Analysis for Collected Data

Here, the data collected as shown above were analyzed using simple-to-use software known as SciDAVis. The data were fed to the software and then graphs were plotted. After that, these graphs for different minerals were compared to ones found on corresponding references and with different other samples of the same species.

Figure 37 in appendix shows usage of the software in the process.

3.2.2 Method of Graphical Interpretation of Raman Spectra Bands for Elemental or Molecular Identification

Here, confirmations and identifications were made through molecular identification by distinctive characteristic Raman shifts and by software (Open Specy) interpretation that has spectral database and a comparison algorithm method.

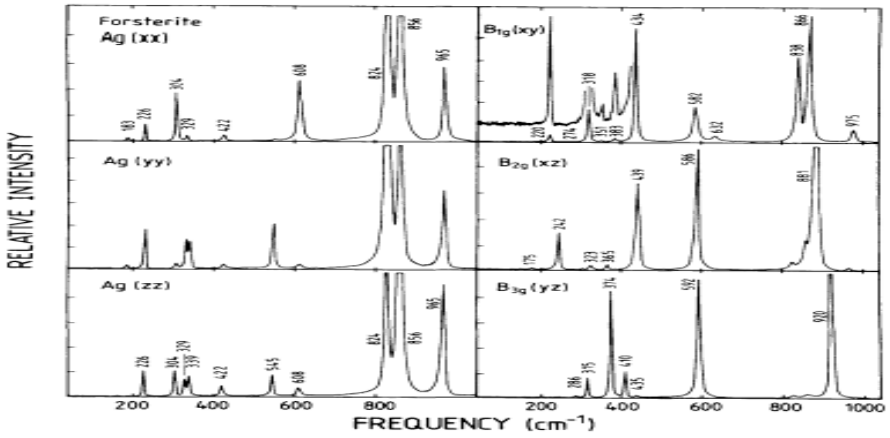

Figure 4: Relative intensity peaks for a mineral (here, forsterite) was shown around a specific Raman shift region (here, around 800 cm^{-1}) (Chopelas, 1991).

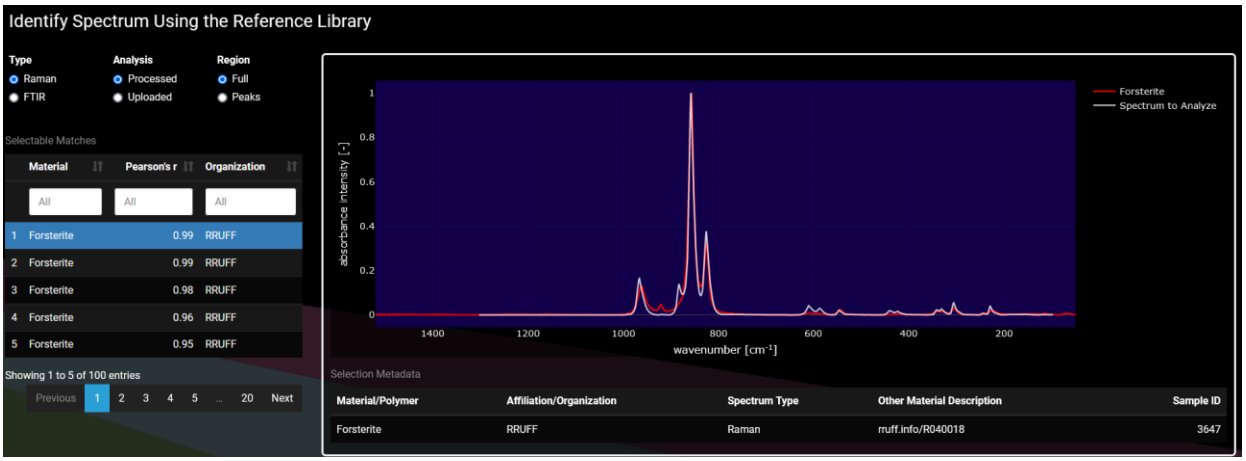

Figure 5: Spectrum identification for forsterite on Open Specy using the reference library.

4. Results and Discussion

4.1 Results

4.1.1Tridymite (SiO_2)

Here, Raman spectra of four tridymite minerals were presented from different four origins; R090042 the Fukang Pallasite meteorite, R090063 Mount Howe 88403 meteorite, R040143 Big Lue Mountain and R160073 synthetic.

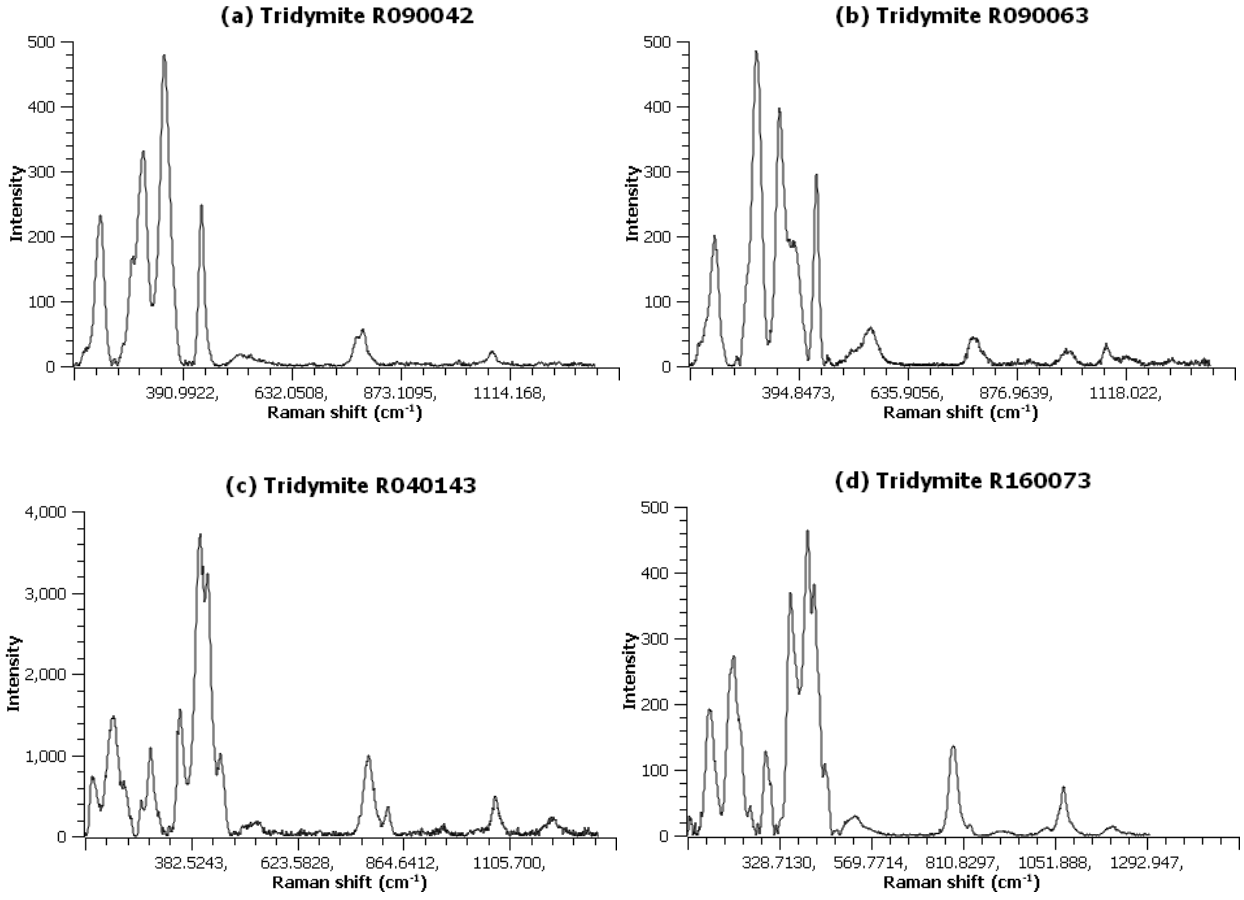

Figure 6: Raman spectra of four different tridymite minerals; (a) the Fukang Pallasite meteorite, (b) Mount Howe 88403 meteorite, (c) Big Lue Mountain and (d) synthetic.

4.1.2 Opal ($SiO_2 \cdot nH_2O$)

Here, Raman spectra of two opal minerals were presented from different two origins; R060652 Ethiopia and X080017 synthetic.

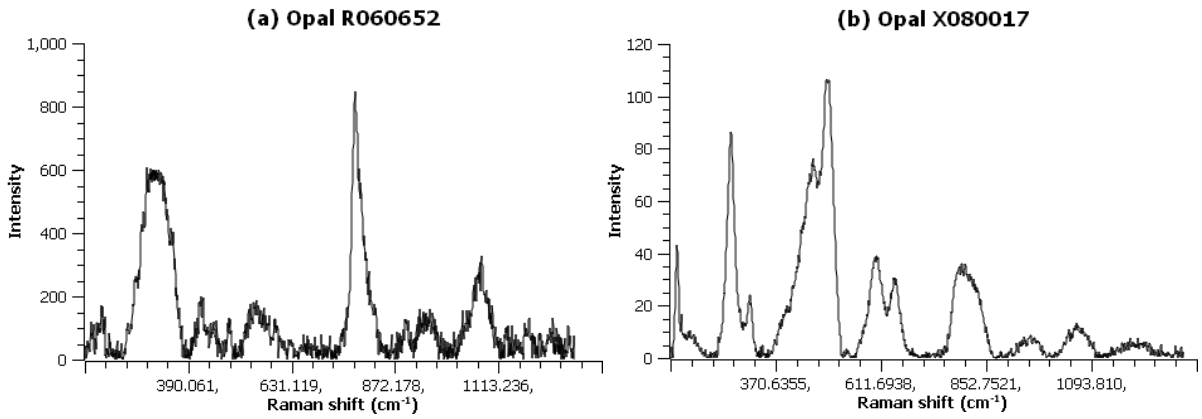

Figure 7: Raman spectra of two different opal minerals; (a) Ethiopia and (b) synthetic.

4.1.3 Cristoballite (SiO_2)

Here, Raman spectra of two cristoballite minerals were presented from different two origins; R061064 Ellora caves, India and X050047 Mayen, Eifel, Germany.

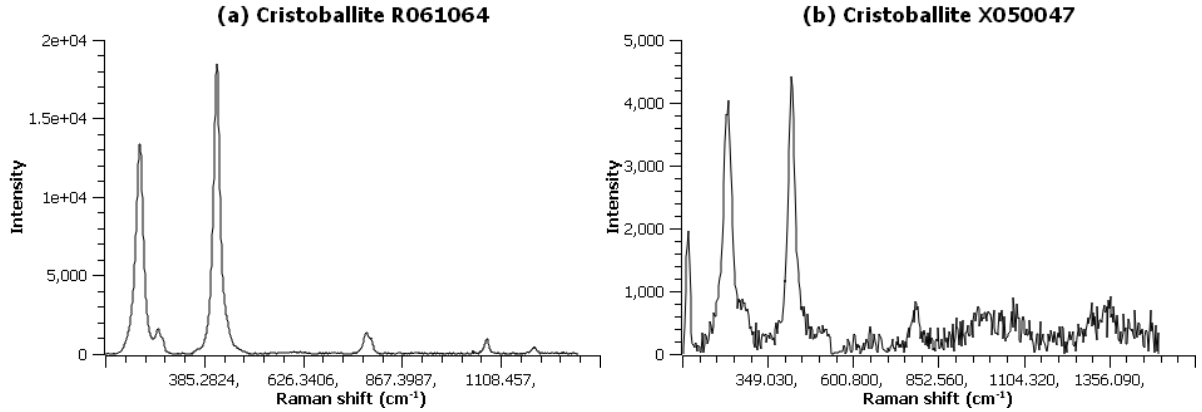

Figure 8: Raman spectra of two different cristoballite minerals; (a) Ellora caves, India and (b) Mayen, Eifel, Germany.

4.1.4 Astrophyllite ($K_2NaFe_7^{2+}Ti_2(Si_4O_{12})_2O_2(OH)_4F$)

Here, Raman spectra of two astrophyllite minerals were presented from different two origins; R060103 Brivik, Norway and R060202 Demix Quarry, Canada.

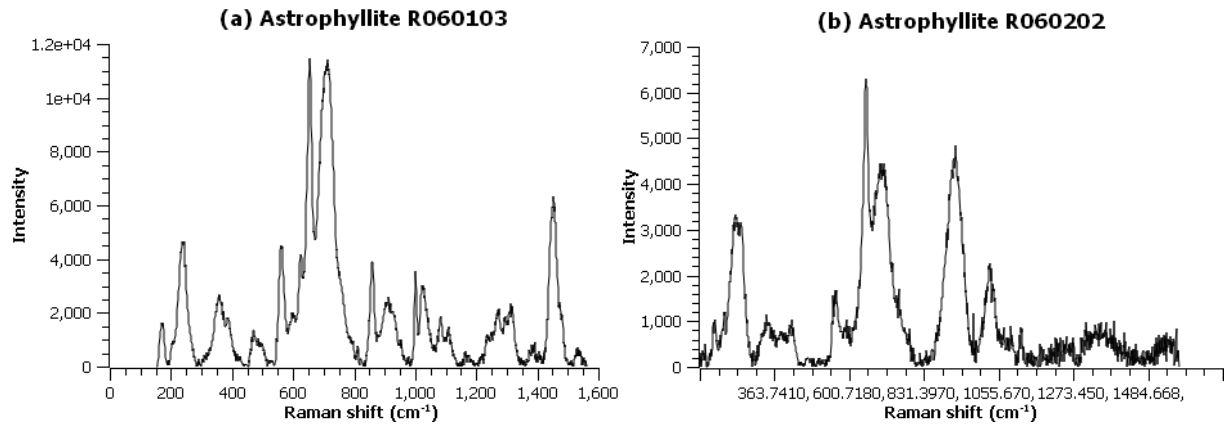

Figure 9: Raman spectra of two different astrophyllite minerals; (a) Brivik, Norway and (b) Demix Quarry, Canada.

4.1.5 Forsterite ($Mg_2(SiO_4)$)

Here, Raman spectra of two forsterite minerals were presented from different two origins; X050081 East Africa and R100099 synthetic.

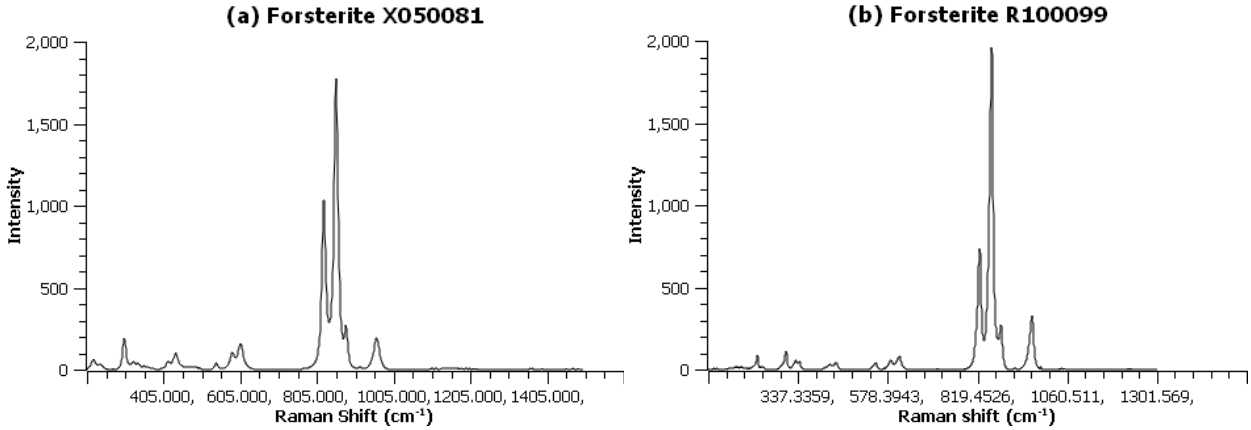

Figure 10: Raman spectra of two different forsterite minerals; (a) East Africa and (b) synthetic.

4.1.6 Fayalite ($Fe_2(SiO_4)$)

Here, Raman spectra of three fayalite minerals were presented from different three origins; X050077 synthetic, R070157 Coso Hot Springs, USA and R100103 Franklin, USA.

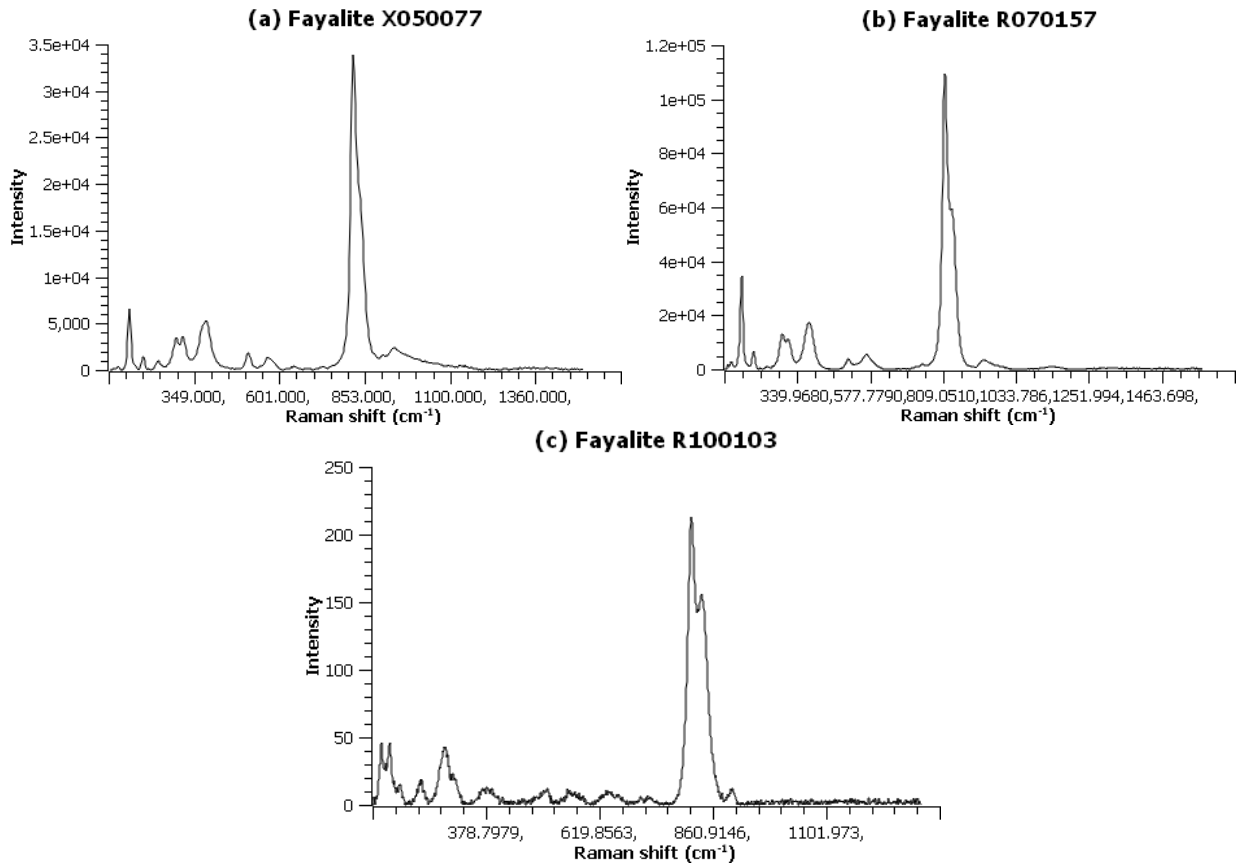

Figure 11: Raman spectra of three different fayalite minerals; (a) synthetic , (b) Coso Hot Springs, USA and (c) Franklin, USA.

4.1.7 Glauberite ($Na_2Ca(SO_4)_2$)

Here, Raman spectra of two glauberite minerals were presented from different two origins; R050350 Soda Lake, USA and R070322 Salton Sea, USA.

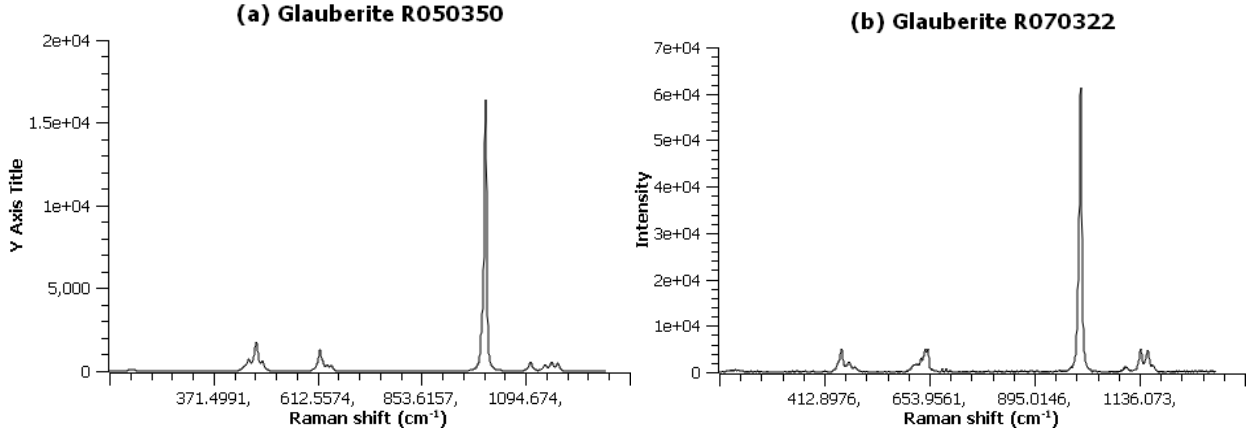

Figure 12: Raman spectra of two different glauberite minerals; (a) Soda Lake, USA and (b) R070322 Salton Sea, USA.

4.1.8 Larnite ($Ca_2(SiO_4)$)

Larnite (RRUFFID = R070530), Larne, County Antrim, Northern Ireland, UK:

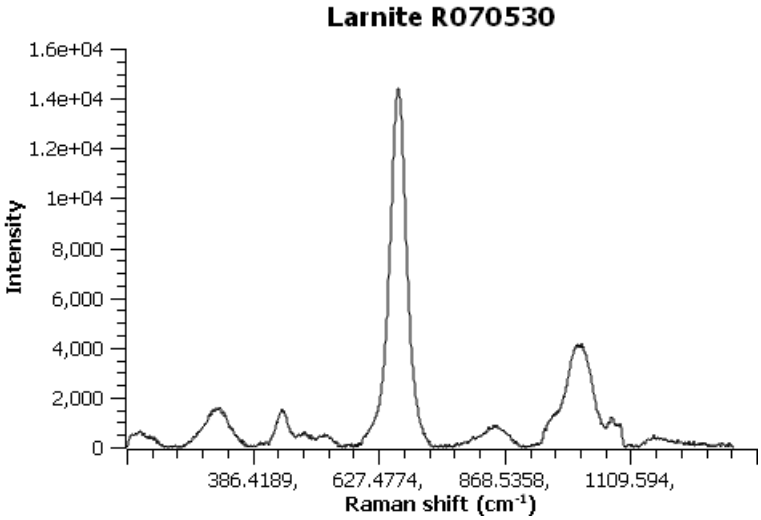

Figure 13: Raman spectrum of Larnite R070530

4.1.9 Monticellite ($CaMg(SiO_4)$)

Here, Raman spectra of two monticellite minerals were presented from different two origins; R040115 Magnet Cove, USA and R100108 Oka, Canada.

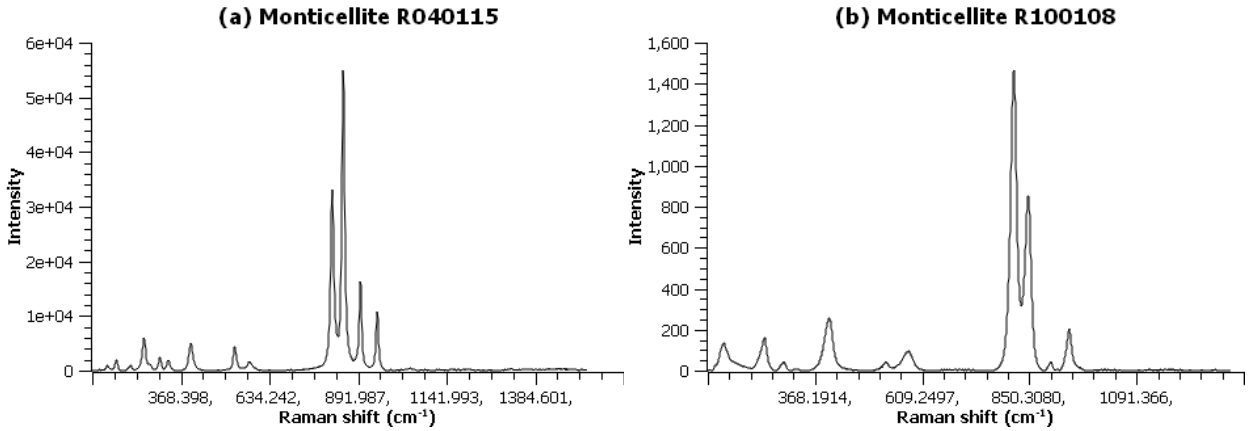

Figure 14: Raman spectra of two different glauberite minerals; (a) Magnet Cove, USA and (b) Oka, Canada.

4.1.10 Kirschsteinite ($CaFe^{2+}(SiO_4)$)

Kirschsteinite (RRUFFID = R070266), Dolores mine, Pastrana, Mazarrón, Murcia, Spain:

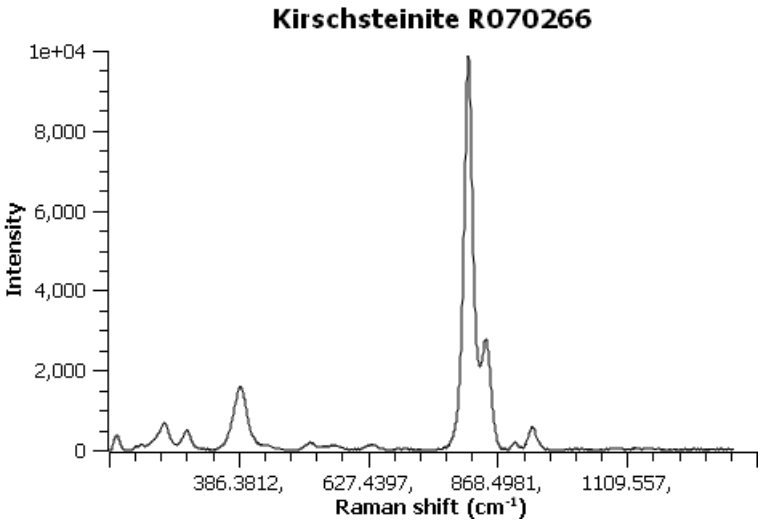

Figure 15: Raman spectrum of Kirschsteinite R070266

4.1.11 Tephroite ($Mn_2^{2+}(SiO_4)$)

Here, Raman spectra of two tephroite minerals were presented from different two origins; R060141 Franklin, USA and R070511 Langban, Sweden.

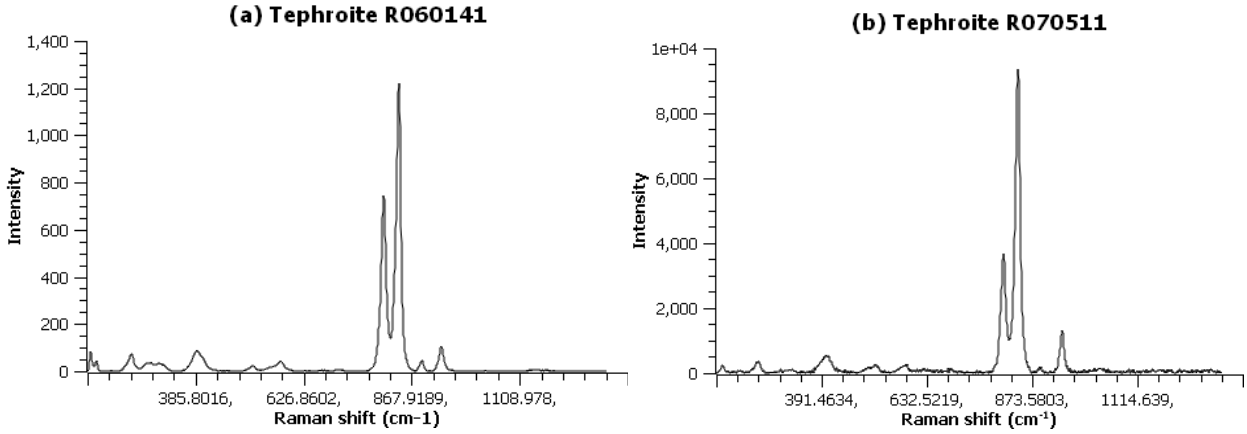

Figure 16: Raman spectra of two different tephroite minerals; (a) Franklin, USA and (b) Langban, Sweden.

4.1.12 Dmisteinbergite ($Ca(Al_2Si_2O_3)$)

Here, Raman spectra of two dmisteinbergite minerals were presented from different two origins; R130085 CV3 type carbonaceous chondrite NWA 2086, Hungary and R130087 Katashina Village, Japan.

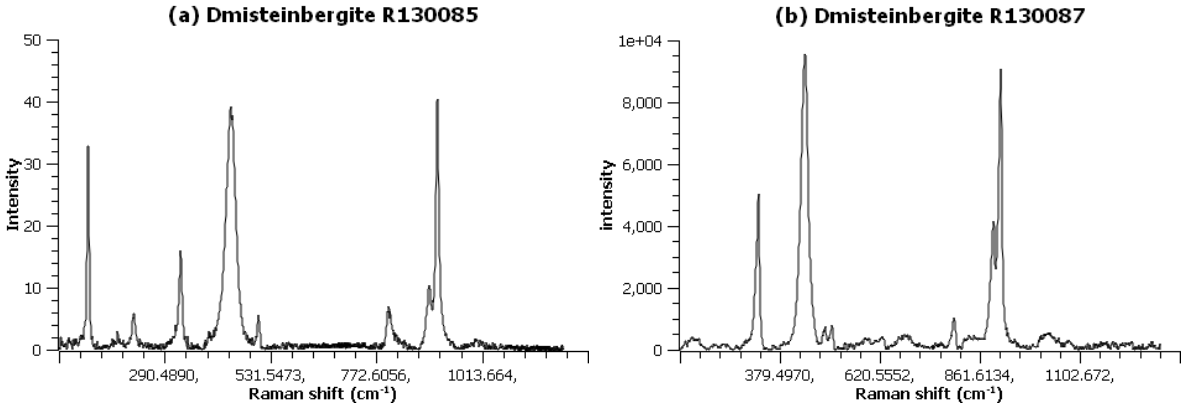

Figure 17: Raman spectra of two different dmisteinbergite minerals; (a) CV3 type carbonaceous chondrite NWA 2086 and (b) Katashina Village, Japan.

4.1.13 Lileyite ($Ba_2Ti_2Na_2Fe^{2+}Mg(Si_2O_7)_2O_2F_2$)

Lileyite (RRUFFID = R140773), Graulay, Hillesheim, Eifel, Rhineland-Palatinate, Germany:

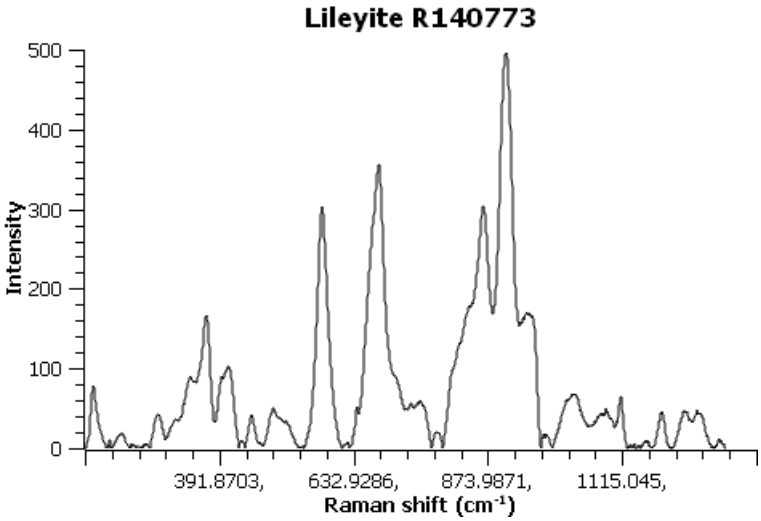

Figure 18: Raman spectrum of Lileyite R140773

4.1.14 Pyroxene

Pyroxene (R110130), Little Deer Creek eclogite, Skagit County, Washington, USA

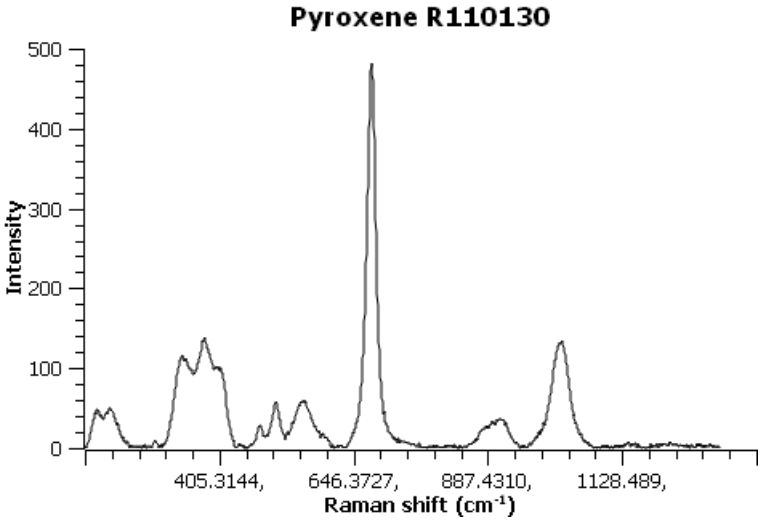

Figure 19: Raman spectrum of Pyroxene R110130

4.1.15 Schorlomite ($Ca_3Ti_2(SiFe_2^{3+})O_{12}$)

Here, Raman spectra of three schorlomite minerals were presented from different three origins; R060125 Magnet Cove, USA, R060349 Sundsvall, Sweden and R140772 Graulay, Germany.

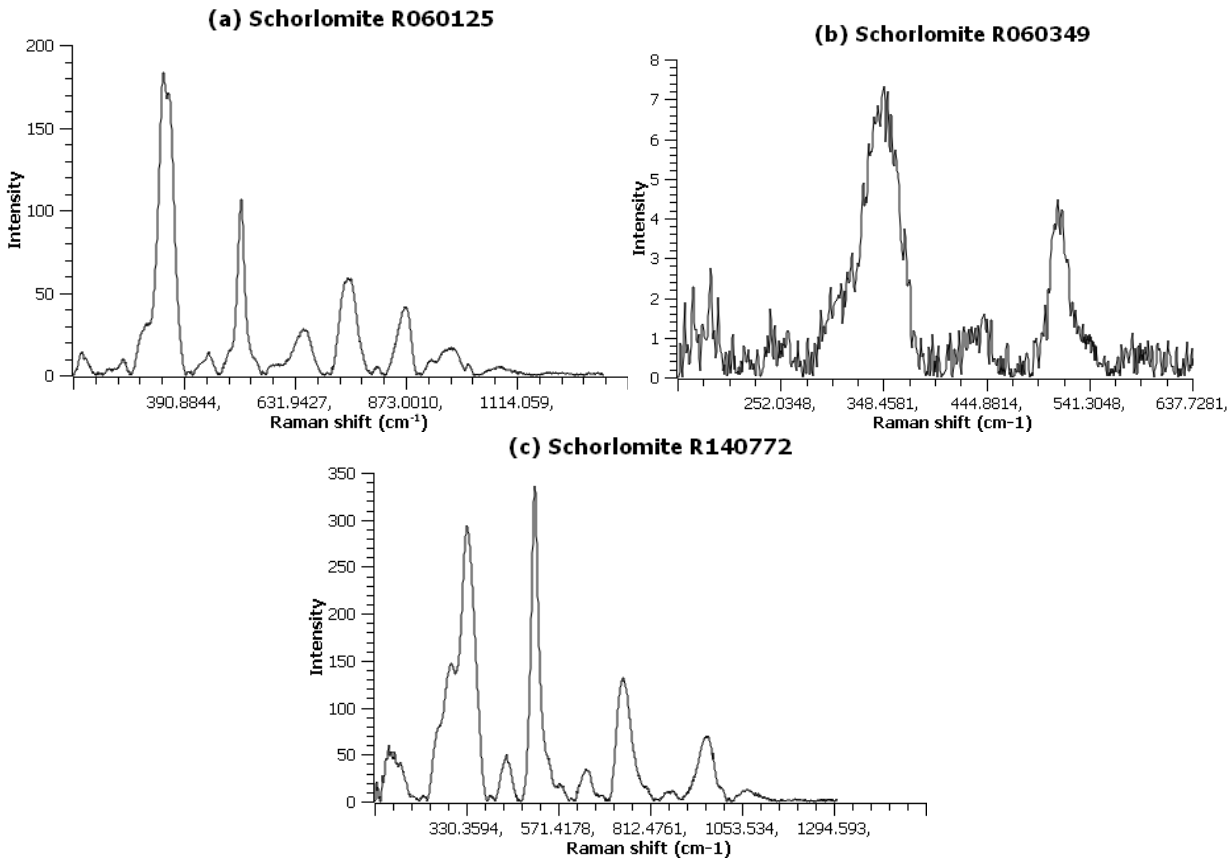

Figure 20: Raman spectra of three different schorlomite minerals; (a) Magnet Cove, USA, (b) Sundsvall, Sweden and (c) Graulay, Germany.

4.2 Discussion

From the results, the majority of spectral peaks for a mineral from different origins were somewhat different from each other in different aspects. For some of them peaks appeared in similar Raman shift ranges but different intensities and for others their intensities appeared to be similar but occur in different Raman shift ranges and for some both differences were observed. These occurred due to line shift problems and the minerals had other impurities and those in a similar mineral group showed additional spectral peaks.

For instance, the silicate cristoballite in Figure 13 showed central peak around 420 cm^{-1} and we could trace its existence in two of our silicate tridymites (R040143 and R160073) and the olivine fayalite in Figure 16 showed central peak around 820 cm^{-1} and we could trace its existence in both of our olivine forsterites because these two minerals come together in some cases.

While data were being collected, it was seen that samples of the majority of our data were further confirmed using X-Ray Diffraction and/or chemical analysis methods by their respective owners and some were only determined by Raman spectroscopy as stated in data collection methods.

But we were able to discuss our results in two of our own discussion methods; Raman peak interpretation and molecular identification by **Open Specy**.

4.2.1 Raman Peak Interpretation

Here, we discussed our results by comparing the relative Raman peak intensities of corresponding minerals found in other studies and we observe the approximate Raman shifts.

Here, we generalized the results in tabular forms that involve minerals with their respective observed peaks (in cm^{-1}) from our results and other reference (s) peaks (in cm^{-1}) from other sources of study.

Note that for peaks in the table below, **VS** stands for **Very Strong**, **S** for **Strong**, **M** for **Medium** and **MS** for **Moderately Small** peaks.

No.	**Mineral**	**RRUFF ID**	**Observed Peaks**	**Reference Peaks from Literature**
1	Tridmite	R090042	350 VS, 304 S, 433 M, 208 M	351 VS, 304 S, 433 S, 209 M, **(Ilieva *et al*.)**
		R090063	301 VS, 352 S, 435 M, 208 MS	350 VS, 455 S, 297 M, 395 MS, **(Kihara *et al.)***
		R040143	403 VS, 420 S, 358 MS, 206 MS	
		R160073	403 VS, 421 S, 358 S, 209 M	
2	Opal	R060652	779 VS, 321 S, 1074 M, 420 MS	292, 363 & 404 VS, 723 & 829 S (**Hatipoglu *et al*.**)
		X080017	492 VS, 268 & 456 S, 602 & 145 M, 805 MS	360 VS, others ranging 750-1650 (**Zaho and Bai**)

3	Cristoballite	R061064	417 VS, 229 S, 274 & 780 MS	420 VS, 230 S (**Zaho and Bai**) 418 VS, 231 S, 114 M (**Ilieva *et al.***)
		X050047	420 VS, 233 S, 115 M, 785 MS, 1074 MS	
4	Astrophyllite	R060103	712 & 654 VS, 1452, 562, 239 & 1000 M, 357, 913 & 1313 MS	870 VS, 718 & 650 S, 565 & 240 M (**Agakhanov *et al***.)
		R060202	653 VS, 926 & 709 S, 238 & 1030 M, 561 MS	

Table 1: Observed Raman spectral peaks (relative intensities) at different Raman shifts of silicate and astrophyllite minerals and their reference peaks from other different studies.

No.	**Mineral**	**RRUFF ID**	**Observed Peaks**	**Reference Peaks from Literature**
1	Forsterite	X050081	855 VS, 823 S, 606 MS, 961 MS	856 VS, 824 VS, 956 M, 608 M **(Chopelas)**
		R100099	858 VS,826 M, 966 MS	859 VS, 830 S **(Mouri and Enami)**
				824 VS, 921 M, 608 M **(Frezzotti *et al*.)**
				800 – 880 high-intensity doublet **(Breitenfeld *et al*.)**
				854 VS, 822 VS, 960 M (**Dyar *et al***.)
2	Fayalite	X050077	820 VS, 840 M, 299 MS, 158 MS	814 VS, 835 M, 289 MS **(Chopelas)**
		R070157	814 VS, 836 M, 290 MS, 155 MS	814 VS, 836 M, 156 MS, 290 MS **(Mouri and Enami)**
		R100103	814 VS, 836 M, 291 MS, 156 MS	

3	Glauberite	R050350	1002 VS, 619 MS, 471 MS	1155 & 1204 VS, 1105 S, 634 & 648 M, 471 & 432 MS **(Lane)**
		R070322	1001 VS, 651 MS, 452 MS	1002 VS, 1106 & 1140 M, 618 & 644 M, 485 MS **(Frezzotti *et al*.)**
4	Larnite	R070530	665 VS, 999 M, 853 MS	814 VS, 840 M, 887 MS, 925 MS (Piriou and McMillan)
5	Monticellite	R040115	850 VS, 818 S, 898 & 948 MS	818 & 851 VS, 949 S, 285 M, 589 & 534 MS **(Chopelas)**
		R100108	816 VS, 848 S, 940 & 255 & 578 MS	818 & 852 VS, 950 S **(Piriou and McMillan)**
6	Kirschsteinite	R070266	815 VS, 846 M, 391 MS	*** No related reference found.**
7	Tephroite	R060141	839 VS, 806 S, 892 & 935 MS	838 VS, 804 S, 891 & 932 MS **(Piriou and McMillan)**
		R070511	841 VS, 808 S, 943 MS	

Table 2: Observed Raman spectral peaks (relative intensities) at different Raman shifts of olivine minerals and their reference peaks from other different studies.

No.	**Mineral**	**RRUFF ID**	**Observed Peaks**	**Reference Peaks from Literature**
1	Dmisteinbergite	R130085	442 & 912 VS, 116 S, 327 & 893 M, 801 & 504 & 221 MS	912 & 442 VS, 327 & 893 M, 504 & 801 MS **(Fintor *et al*.)** 914 & 442 VS, 330 &896 M, 801 MS **(Nestola *et al*.)**
		R130087	440 &912 VS, 327 & 895 M, 800 & 505 MS	
2	Lileyite	R140773	907 VS, 679 & 866 & 577 S, 944 & 369 M, 408 & 753 & 166 MS	*** No related reference found**.
3	Pyroxene	R110130	679 VS, 1021 & 379 & 339 M, 921 & 561 &	Orthopyroxene (1006, 678, 660) and clinopyroxene (1005, 665)

			209 MS	**(Wang *et al*.)**
4	Schorlomite	R060125	347 & 357 VS, 515 S, 747 & 873 M, 651 & 169 MS	*** No related reference found.**
		R060349	349 & 754 VS, 512 M, 187 & 862 & 950 MS	
		R140772	510 VS, 332 S, 742 & 292 M, 964 & 126 & 435 MS	

Table 3: Observed Raman spectral peaks (relative intensities) at different Raman shifts of pyroxene minerals and their reference peaks from other different studies.

4.2.2 Molecular Identification by "Open Specy"

Here, we discuss what we found by feeding our Raman spectral data into the Open Specy analyzer website and then the software identifies what type of element or molecule was used in the data. Moreover, it compares it with the ideal peak characteristics and matches from scale of 0 to 1, that is, 0% to 100%.

Note that the **red** line represents ideal peaks for that mineral according to the reference library and the **white** line represents observed peaks from our RRUFF data.

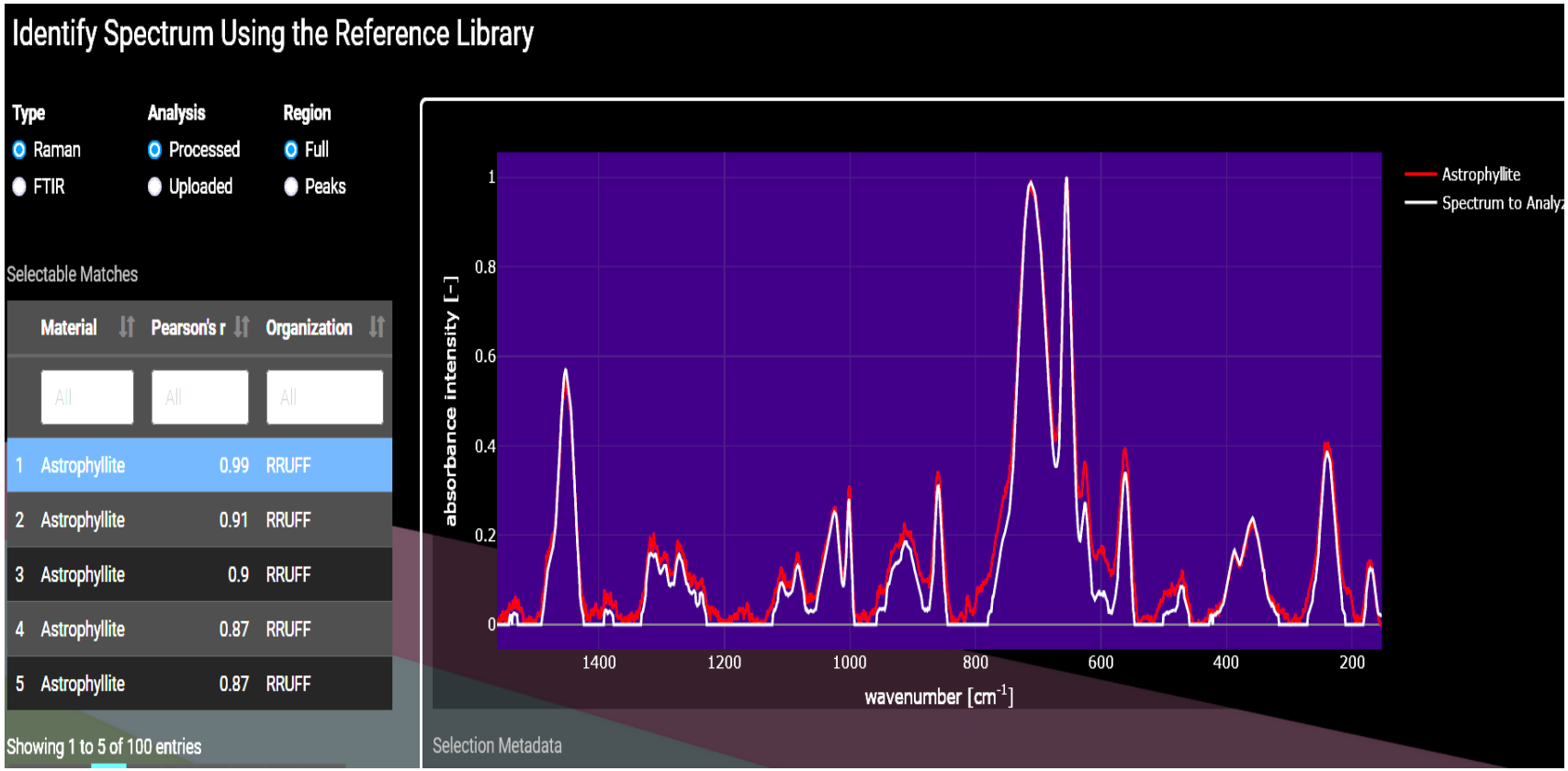

Figure 21: Astrophyllite R060103 matched 99% with the ideal spectrum.

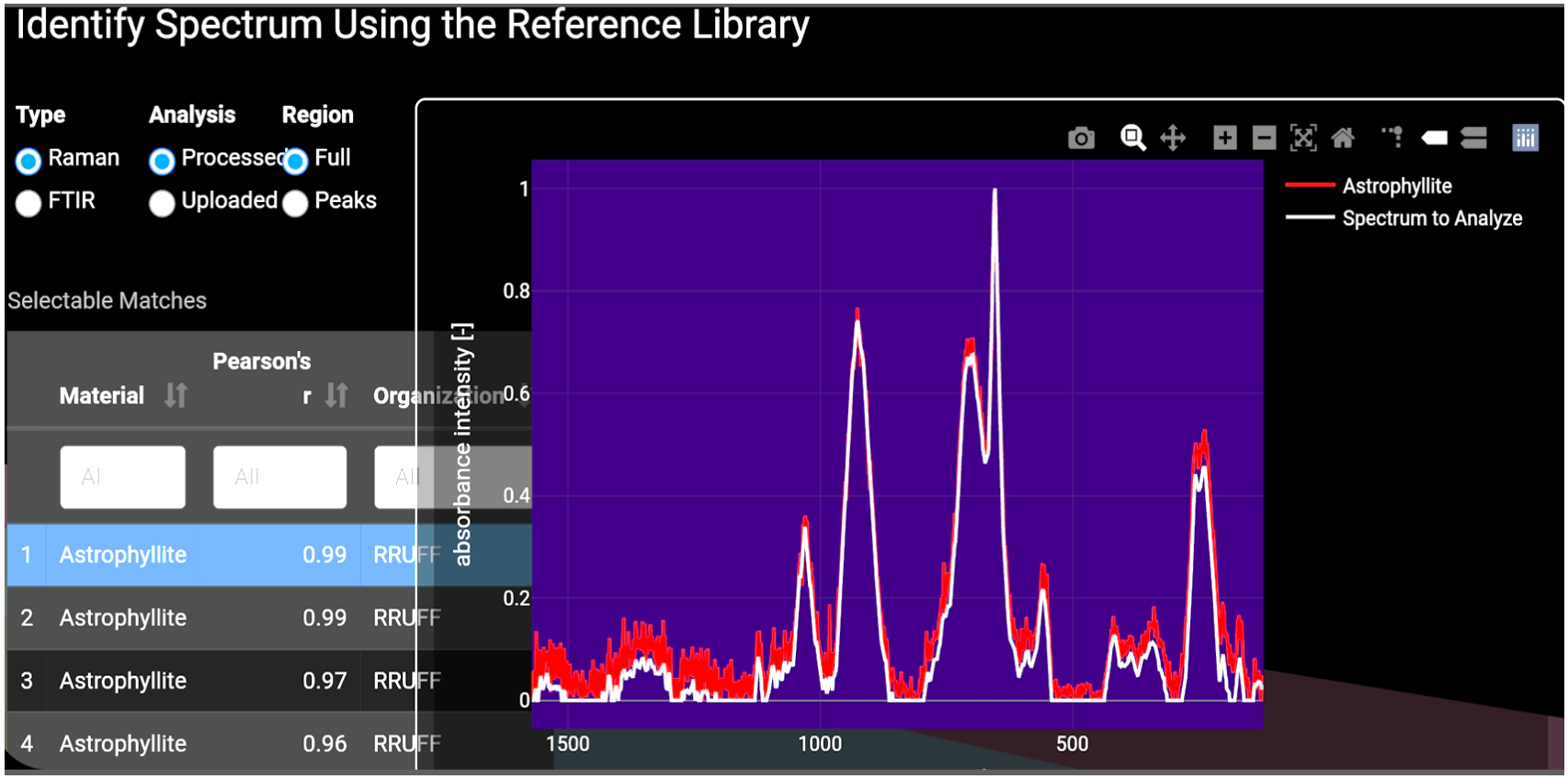

Figure 22: Astrophyllite R060202 matched 99% with the ideal spectrum.

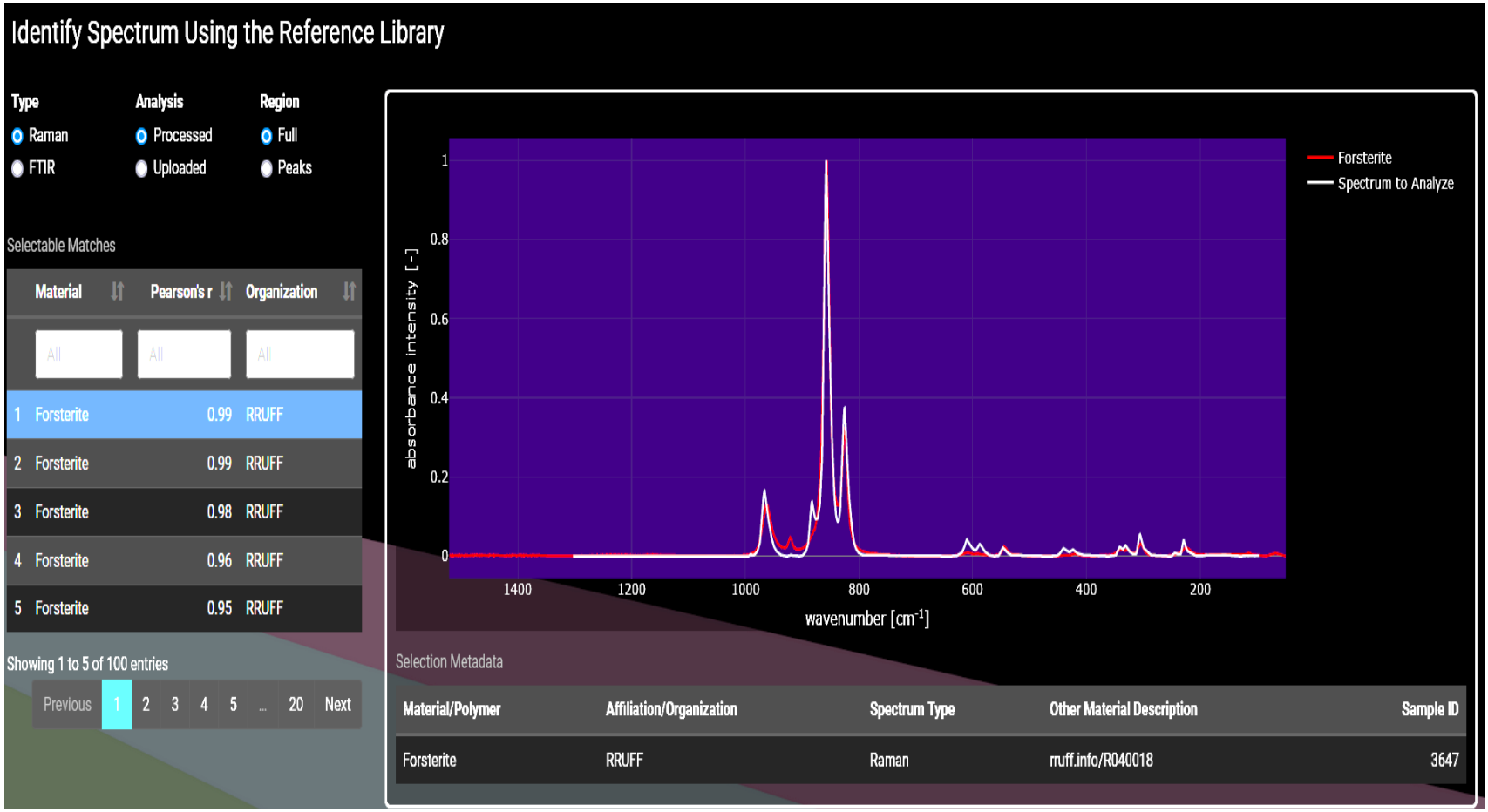

Figure 23: Forsterite X050081 matched 99% with the ideal spectrum

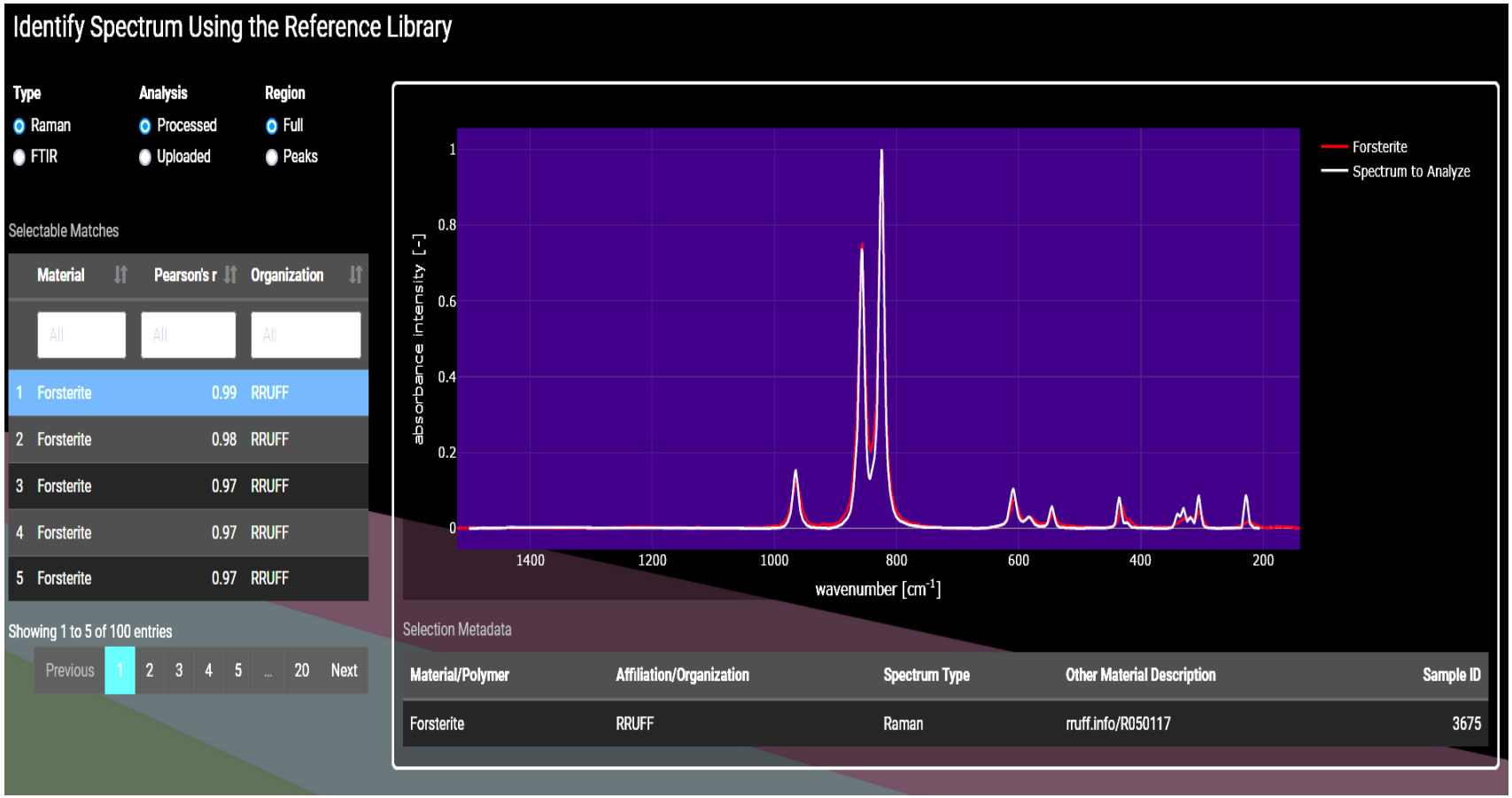

Figure 24: Forsterite X050080 matched 99% with the ideal spectrum.

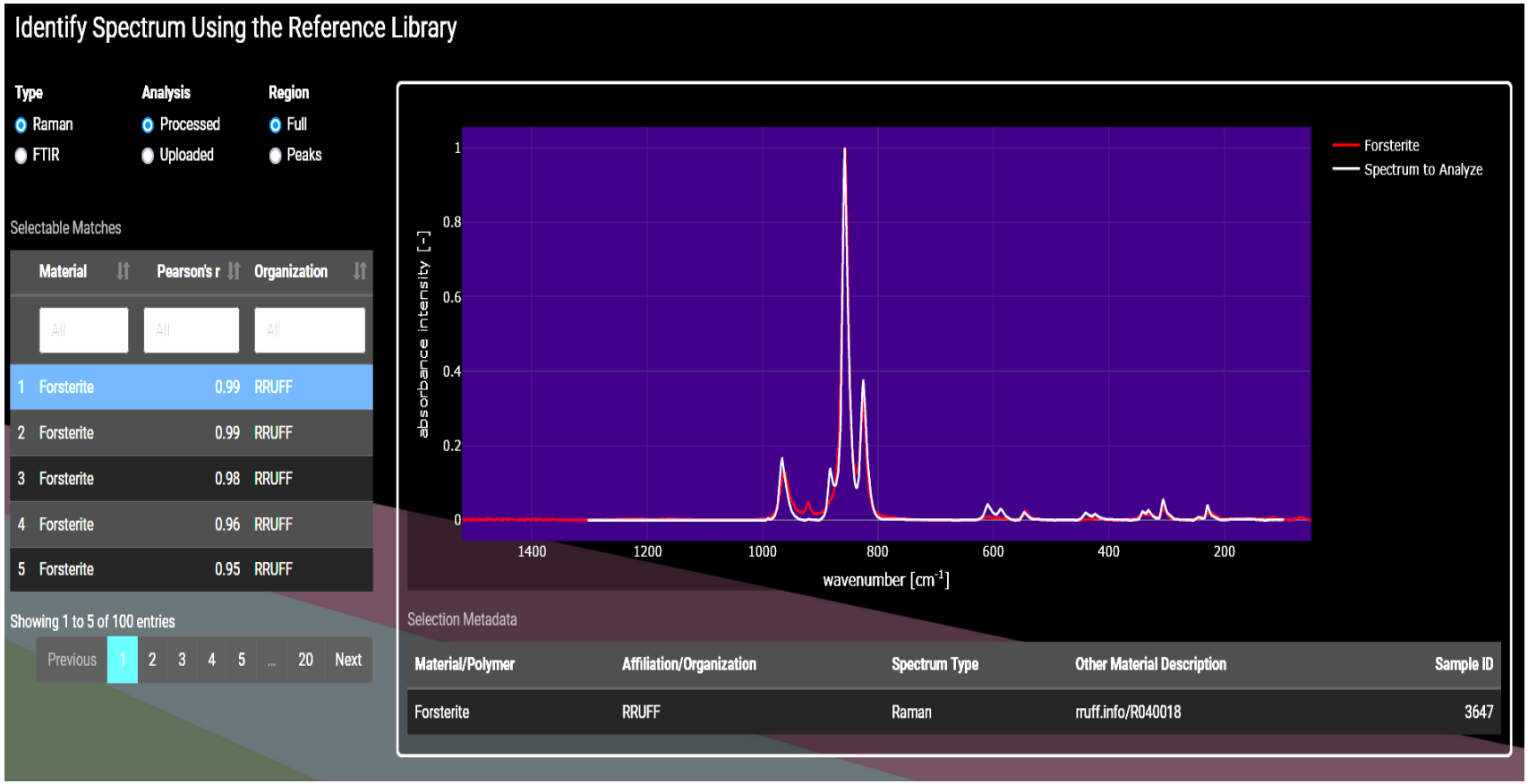

Figure 25: Forsterite R100099 matched 99% with the ideal spectrum.

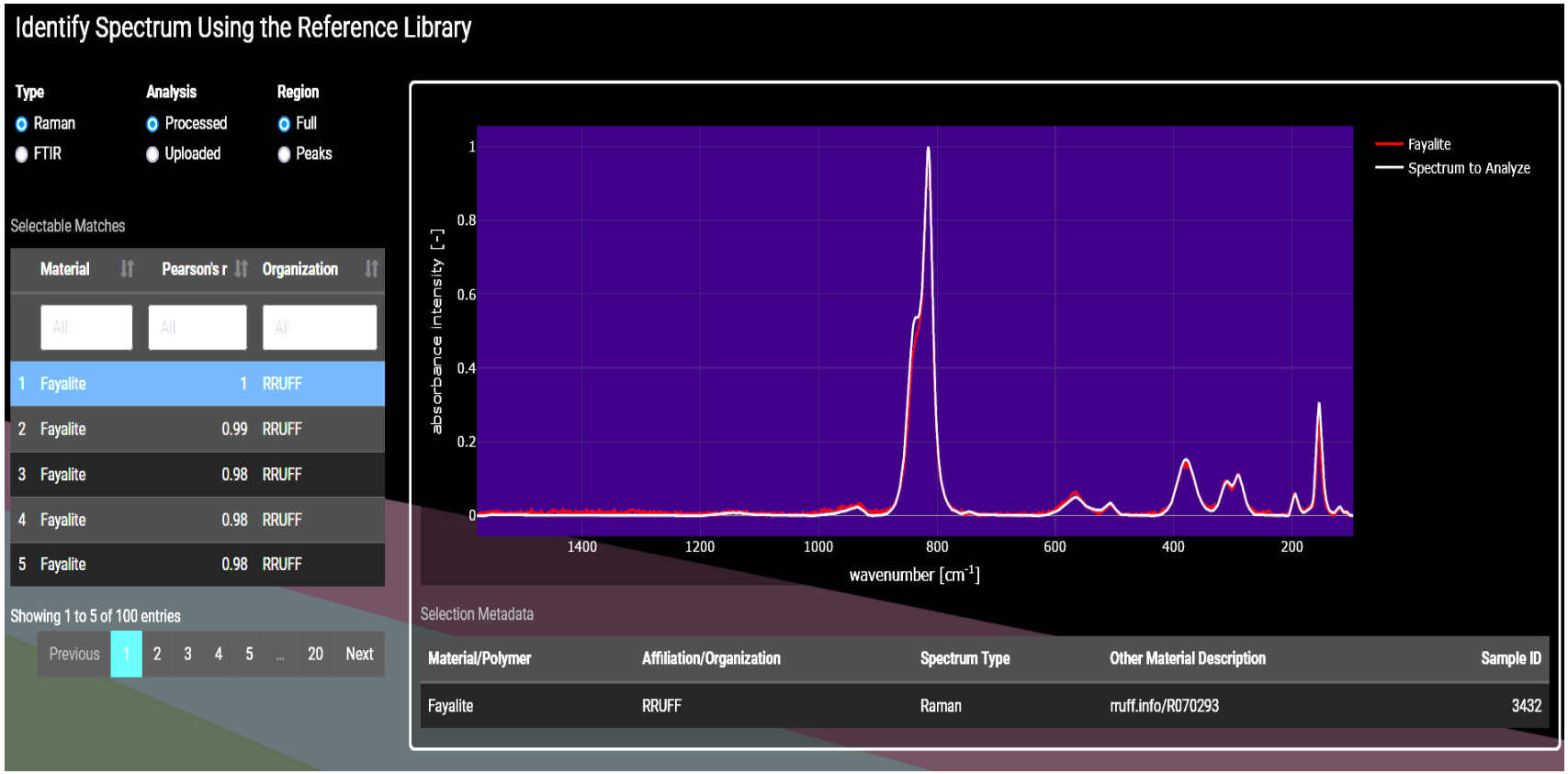

Figure 26: Fayalite R070157 matched 100% with the ideal spectrum.

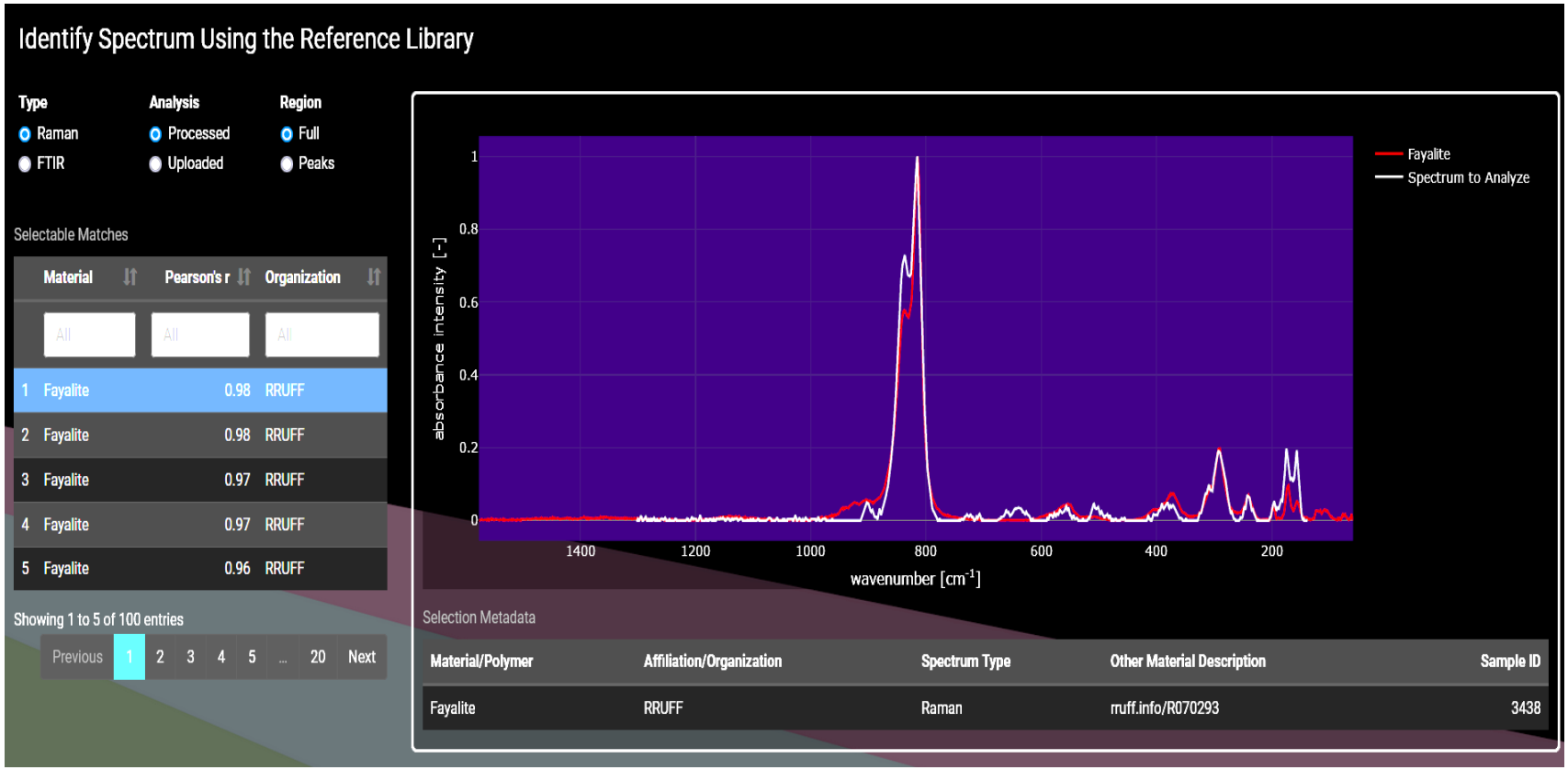

Figure 27: Fayalite R100103 matched 98% with the ideal spectrum.

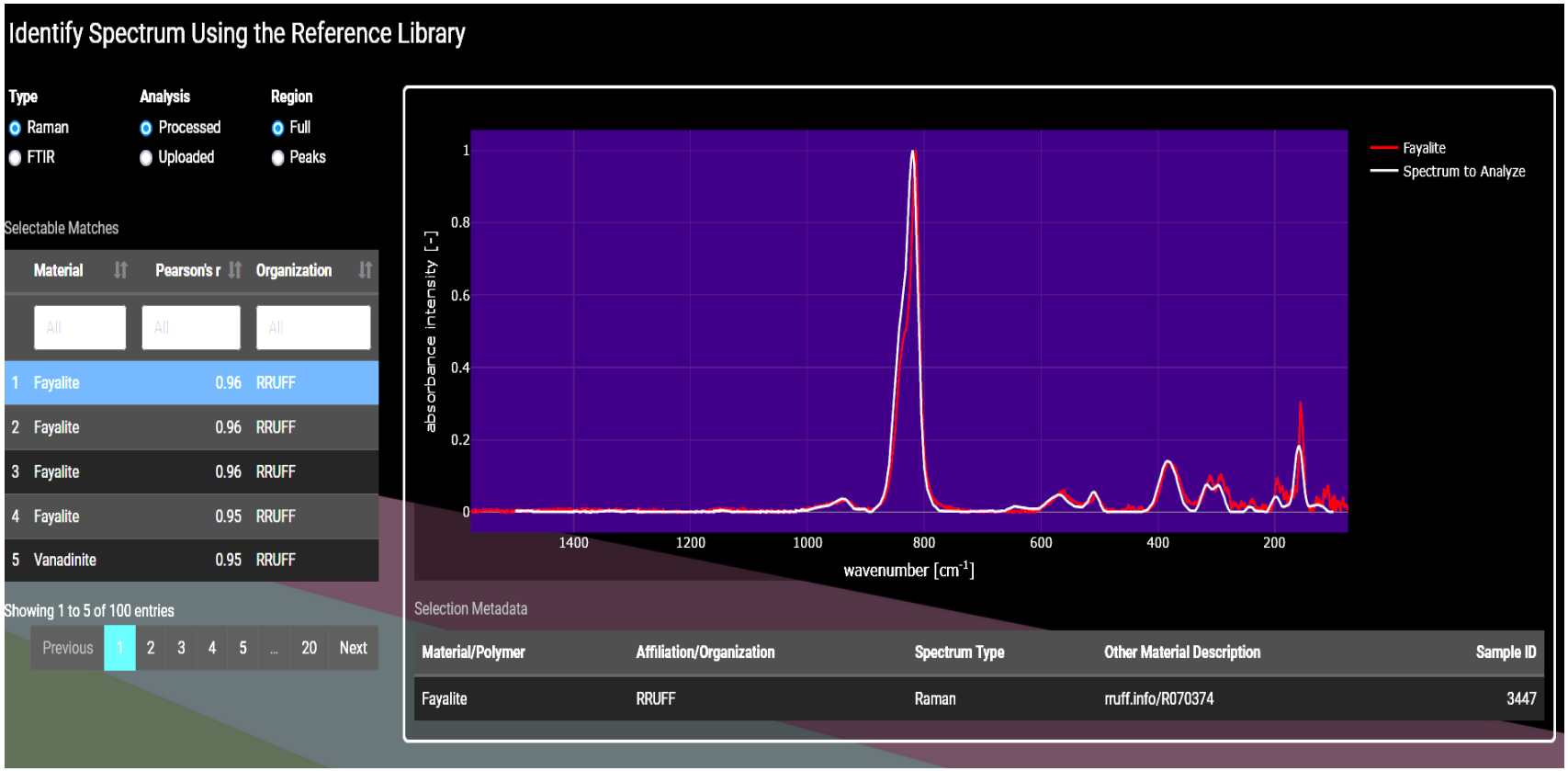

Figure 28: Fayalite X050077 matched 96% with the ideal spectrum.

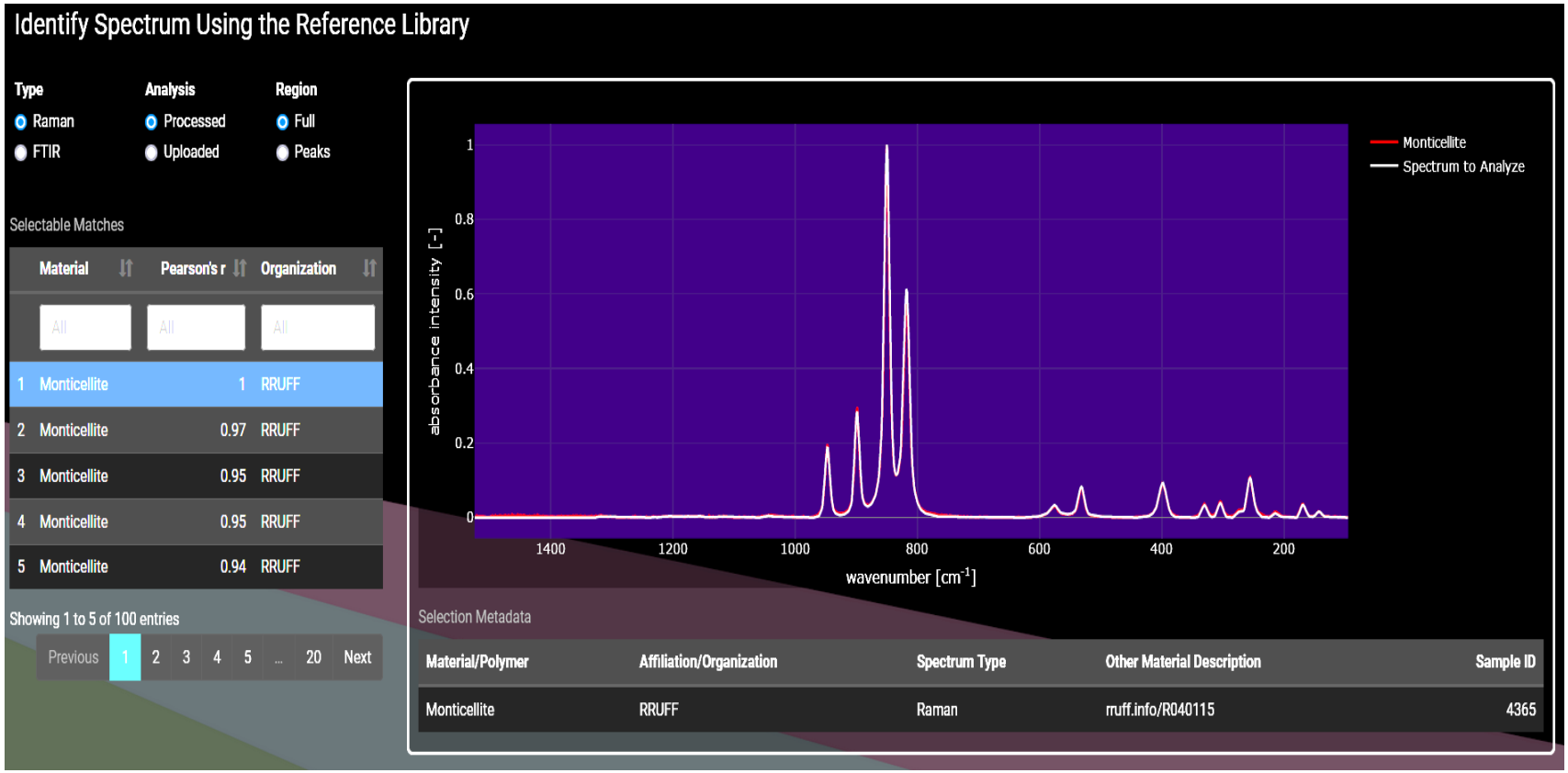

Figure 29: Monticellite R040115 matched 100% with the ideal spectrum.

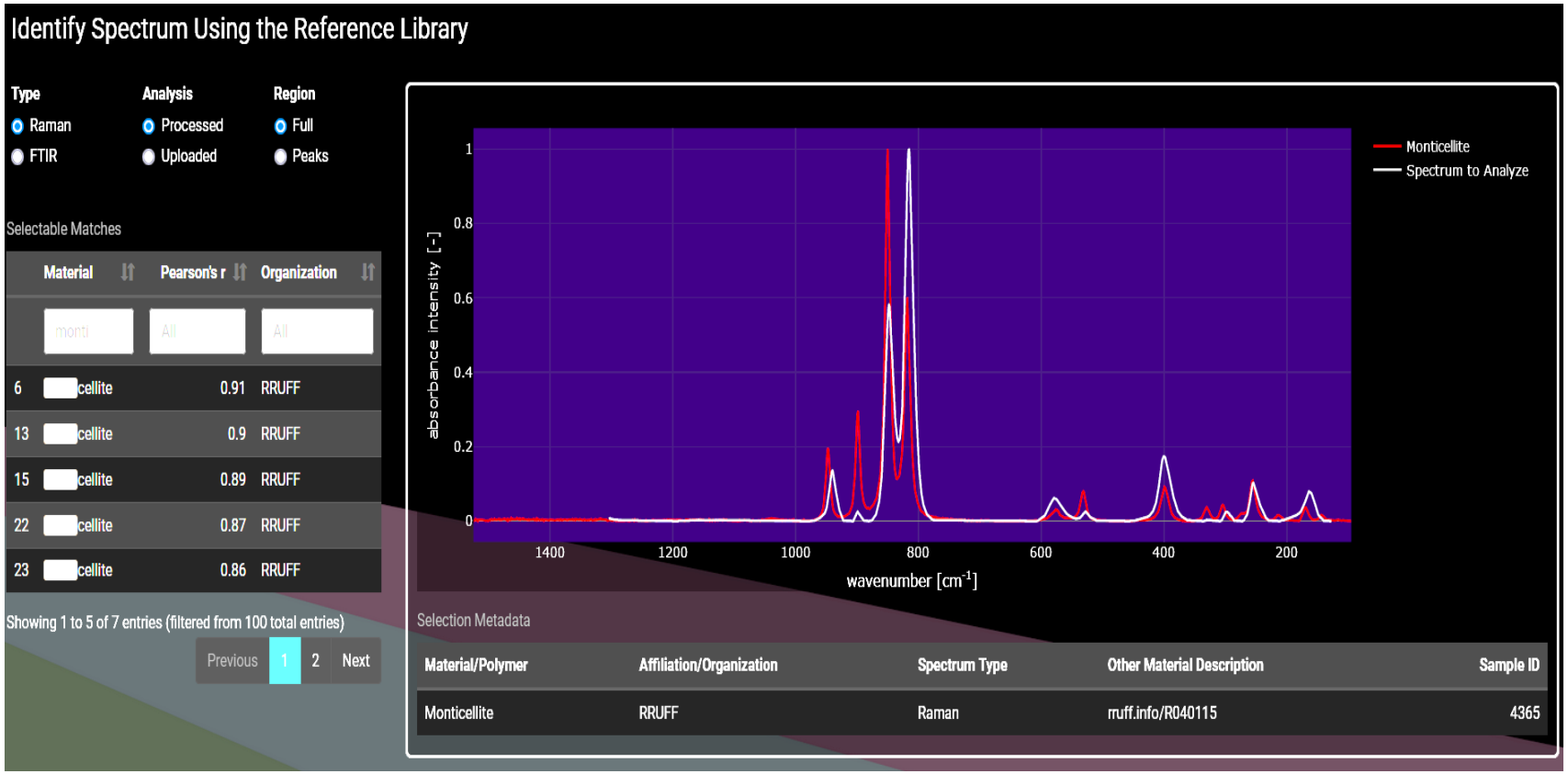

Figure 30: Monticellite R100108 matched 91% with the ideal spectrum.

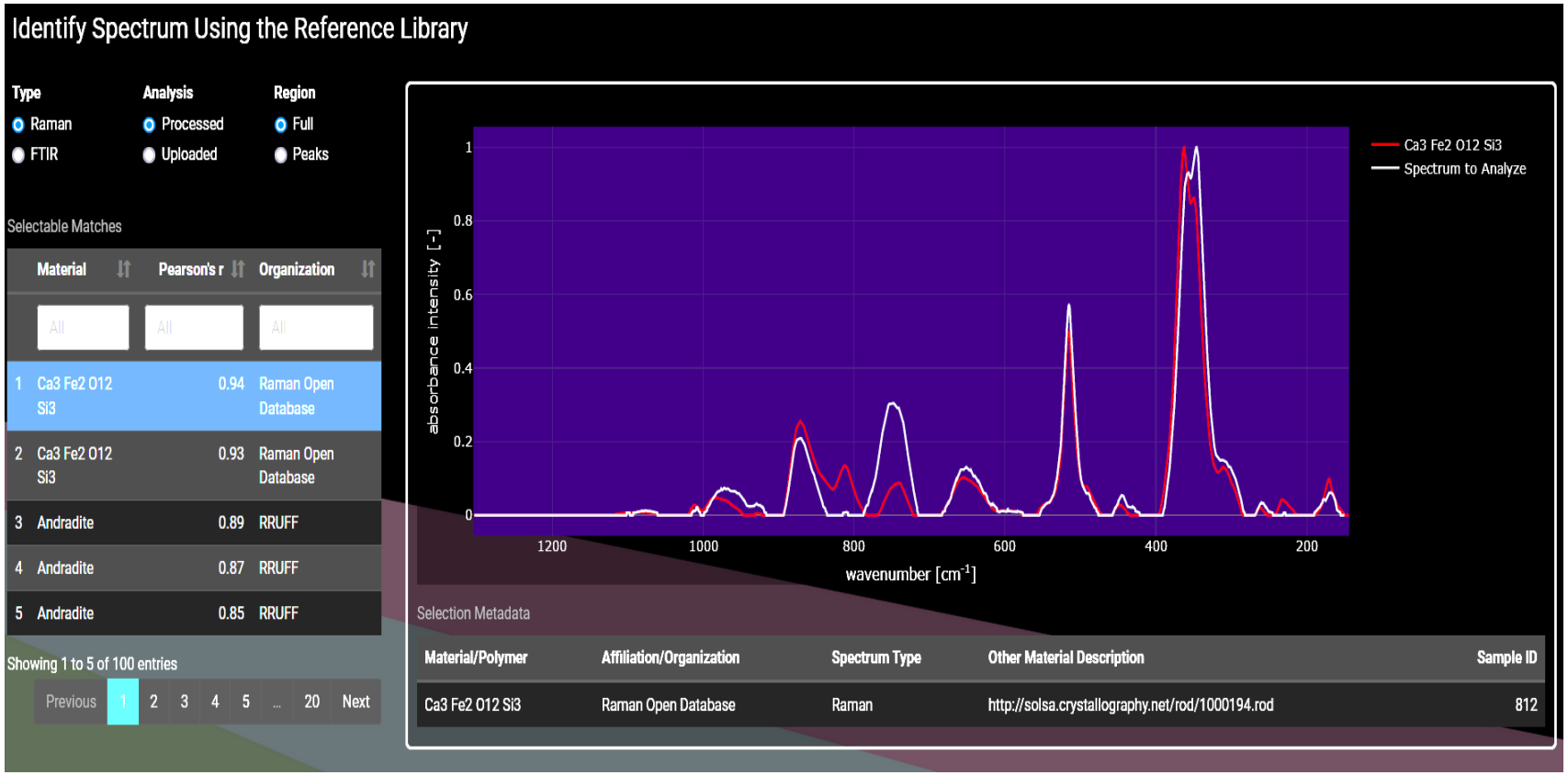

Figure 31: Schorlomite R060125 matched 94% with the ideal spectrum.

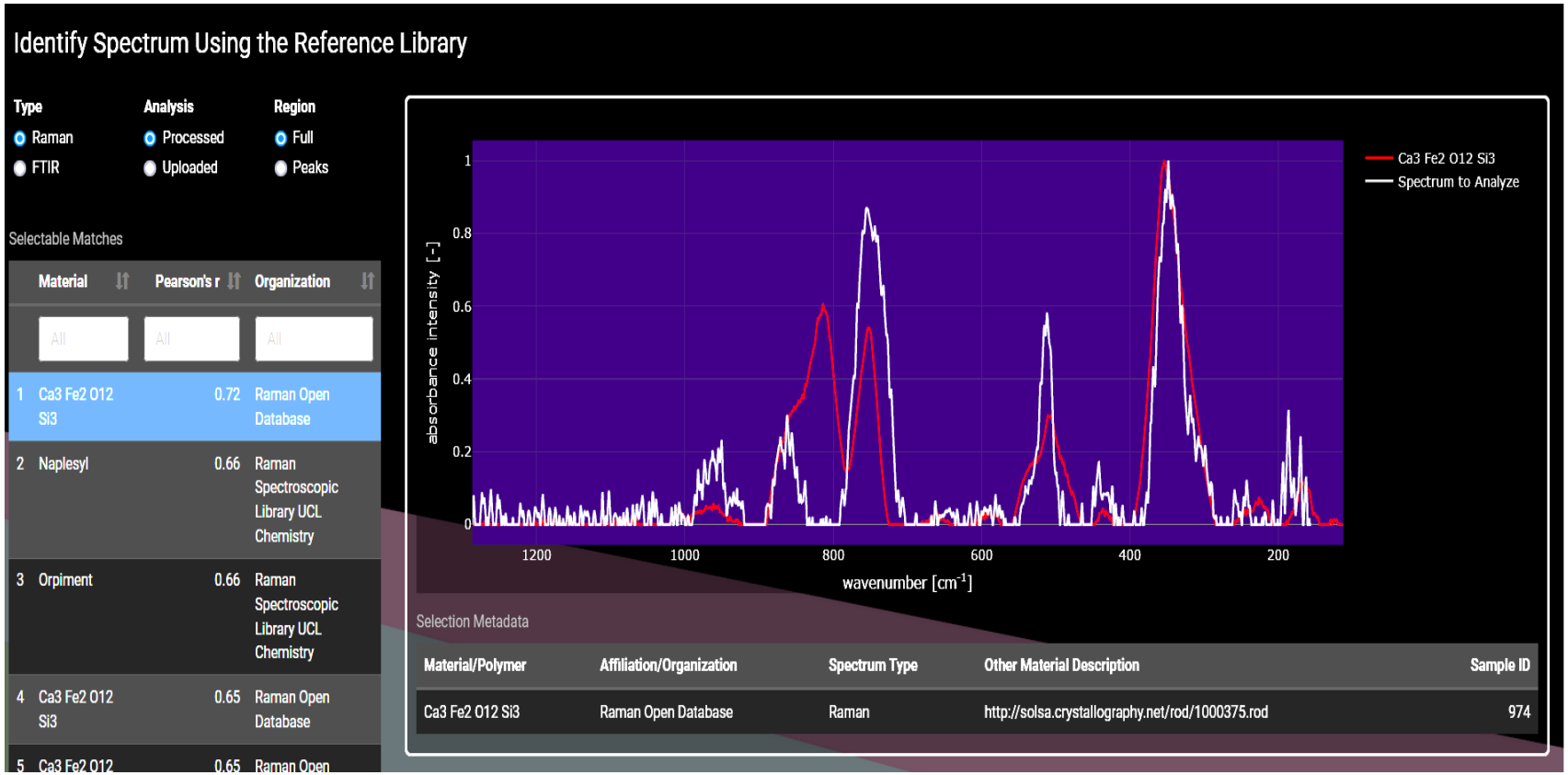

Figure 32: Schorlomite R060349 matched 72% with the ideal spectrum.

Here, we showed that some of the mineral data could be identified in Open Specy, for most of them with > 90% match with ideal spectrum and only one (Schorlomite R060349) 72% match.

5. Conclusions and Recommendation

5.1 Conclusions

In this thesis, the intensity of scattered laser light through a sample medium and wavenumber or Raman shifted lines were focused for Raman data analysis methods. These parameters (intensity and wavenumber) were the targets of this study because their XY line graphs result our desired Raman spectra to be analyzed latter.

RRUFF data were taken for different targeted minerals of groups such as olivines, pyroxenes, silicates and others with astronomical relations and analogues. Fifteen minerals were targeted with astronomical relations such as **Tridymite, Opal, Cristoballite, Astrophyllite, Forsterite, Fayalite, Glauberite, Larnite, Monticellite, Kirschsteinite, Tephroite, Dmisteinbergite, Lileyite, Pyroxene,** and **Schorlomite**. The Raman spectra of these individual minerals from different sources were investigated by plotting intensity vs. wavenumber (Raman shift) graphs using a software called **SciDAVis**. The results revealed that the spectral peaks observed from graphs were found to be close to their corresponding reference and ideal peaks in two ways.

The first identification method used was to compare relative spectral peaks in other different studies or literature with our relative intensity peaks from the resulting plots. Majority of our peaks were seen to appear analogous to peaks of other studies. That means, relative intensity peaks appeared in regions of Raman shifts as expected and indicated in literatures and studies. However, some of our results did not match with others for some suspected reasons such as instrumental problems, sample impurities and/or line broadening, and no related reference peaks from other studies were found for some minerals such as **Kirschsteinite, Lileyite and Schorlomite**, thus, this study provided better organized Raman spectra of minerals of the cosmos and a better compiled document regarding this issue that any future researcher can use in reference to.

Since secondary data were taken, we were not sure to tell which of these reasons were causes of these line shifts. But according to many studies, line broadening is the major factor in line shifts, which is the spreading across a greater wavelength range of absorption lines (dark) or emission

(bright) lines in the radiation received from the sample so the possible cause might be this case for most of the deviations.

For instance, two of our Tridymite plots (from Fukang Pallasite meteorite in China and Mount Howe 88403 meteorite) were very similar to their respective comparisons and the other two (from Big Lue Mountain, USA and synthetic) seem to have deviated from reference peaks as shown in table 1.

The second identification method used was to feed our Raman data for all minerals to the website **Open Specy** and see if our Raman lines matched the ideal ones that the developers put. Unfortunately, the majority of our Raman data of minerals could not find any match in this website except for some minerals such as **Astrophyllite**, **Forsterite**, **Fayalite**, **Monticellite** and **Schorlomite** with matches of above 90% for most. But the reasons we could not find matches were that most of the minerals were not included in the database of **Open Specy** due to their rarity and line shifts (broadenings) of these data.

Generally, from these results, we can conclude that the majority of our Raman spectra matched the expected and ideal results and the rest resembled reference peaks. Thus, Raman spectroscopy can be used to study mineralogy of celestial bodies from minerals of Earth analogy and meteorite samples.

5.2 Recommendation

The use of Raman Laser Spectroscopes (RLS) in Astronomical applications has been a trending research area in developed nations for a few decades. Studying minerals by RLS has shown promising results in identifying their species with greater precision than any other spectroscopic method we use in Astronomy. Even though RLS is expensive to use for developing nations like Ethiopia, we can begin our journey from here in building the sector and enriching our scientific community with knowledge of the Solar System.

This work investigated how RLS can be applied in studying mineralogy of celestial bodies from Raman data of meteorites and Earth analogues from databases. Thus, we strongly recommend both future researchers and institutes to further study this area by analyzing our own mineral or

meteoritic samples using the spectroscope for ourselves, which will help us gaining more work experience in this area of study.

Research Fund Acknowledgment

This research project is funded by Adama Science and Technology University under the grant number ASTU/SM-R/306/21 Adama, Ethiopia.

6. References

Adamo, T. (2021). Understanding Raman Spectroscopy. *Traces Center*. https://www.utsc.utoronto.ca/~traceslab/PDFs/raman_understanding.pdf/

Agakhanov, A., Pautov, L., and Karpenko, V. (2016). Two Astrophyllite Supergroup Minerals: Bulgakite, a New Mineral from the Darai-Pioz Alkaline Massif, Tajikistan and Revision of the Crystal Structure and Chemical Formula of Nalivkinite. *Canadian Mineralogist*. **10**:24-26.

Agle, C., Brown, D., Bauer, M. (2014). Rosetta's Comet Target 'Releases' Plentiful Water. NASA. Retrieved on December 28, 2020.

Amos, J. (2012). Nasa's Curiosity Rover Lifts its Navigation Cameras. *BBC News.* Retrieved on December 27, 2020.

Angel, M., & Gomer, N. (2011). Remote Raman. Columbia: *focal point review.*

Beegle, L., Bhartia, R.,DeFlores, L., Darrach, M., Kidd, R., Abbey, W., Asher, S. (2014). SHERLOC: Scanning Habitable Environments With Raman & Luminescence for Organics & Chemicals, an Investigation for 2020. *International GeoRaman Conference*. **11**:1.

Breitenfeld, L., Dyar, M., Carey, C., Tague Jr., T., Wang, P., Mullen T., and Parente M. (2018). Predicting Olivine Composition using Raman Spectroscopy through Band Shift and Multivariate Analyses. *American Mineralogist*.

Chopelas, A. (1991). Single Crystal Raman Spectra of Forsterite, Fayalite, and Monticellite. *American Mineralogist*. **76**:1101-1109.

Dustin, W., Faris S., and Ioan N. (2017). Raman spectroscopy: Techniques and applications in the life sciences. Nottingham: *Optical Society of America.*

Dyar, M., Carey, CJ., Breitenfeld, L., Bartholomew, P., Tague, T., Wang, P., Mertzmann, S., Byrne, S., Crowley, M., Leight, C., and Watts, E. (2016). Quantifying Mineral

Abundances in Mixtures using Raman Spectroscopy: Calculating Raman Coefficients using a Diamond Reference. 47th *Lunar and Planetary Science Conference*. **2106**.

Fintor, K., Park, C., Nagy, S., Pal-Molnar, E., And Krot, A. (2014). Hydrothermal Origin of Hexagonal $Caal_2si_2o_8$ (Dmisteinbergite) in a Compact Type A CAI from the Northwest Africa 2086 CV3 Chondrite. *Meteoritics & Planetary Science*. **49**(5):812–823.

Frezzotti, M., Tecce, F., and Casagli, A. (2012). Raman Spectroscopy for Fluid Inclusion Analysis. *Journal of Geochemical Exploration*. **112**:1-20.

Frost, R., Palmer, S., Bouzaid, J., and Reddy, J. (2007). A Raman spectroscopic study of humite minerals. *Journal of Raman Spectroascopy*. **38**(1).

Greaves, J., De Vries, L.; Acke, B., Blommaert, L., Waelkens, C., Waters, M., Vandenbussche, B., Min, M., Olofsson, G., Dominik, C., Decin, L., Barlow, J., Brandeker, A., Di Francesco, J., Glauser, M., Harvey, M., Holland, S., Ivison, J., Liseau, R., Pantin, E., Pilbratt, L., Royer, P., Sibthorpe, B. (2012). Comet-like mineralogy of olivine crystals in an extrasolar proto-Kuiper belt. *Nature*. **490** (7418): 74–76.

Hänni, H., Kiefert, L., and Chalain, JP. (1997). A Raman Microscope in the Gemmological Laboratory: First Experiences of Application. *J. Gemm*. **25**(6).

Hatipoglu, M., Kibici, Y., Yanik, G., Ozkul, C., Demirbilek, M. and Yardimci, Y. (2015). Nano-structure of the Cristobalite and Tridymite Stacking Sequences in the Common Purple Opal from the Gevrekseydi Deposit, Seyitömer-Kütahya, Turkey. *Oriental Journal of Chemistry*. **31**(1):45-46.

Hoefen, M., *et al*. (2003). Discovery of Olivine in the Nili Fossae Region of Mars. *Science.* **302**. *doi*:*10.1126/science.1089647*.

Huang, E., Chen, C., Huang, T., Lin, E., and Xu, J. Raman spectroscopic characteristics of Mg-Fe-Ca pyroxenes. (2000). *American Mineralogist*. **85**:473–479.

Ilieva, A., Mihailova, B., Tsintsov, Z., and Petrov, O. (2007). Structural State of Microcrystalline Opals: A Raman Spectroscopic Study. *American Mineralogist*. **92**: 1325-1333.

Jorge, V., Frances, W., Andrew, C., Ralf, J., Oleg, K., Vale´rie, C., Igor, M., *et al*. (2017). Habitability on Early Mars and the Search for Biosignatures with the ExoMars Rover. *Astrobiology.* **17**(6 &7): 493

Kayama, M., Nagaoka, H., and Niihara, T. (2018). Lunar and Martian Silica. *Minerals*. **8** (267).

Kihara, K., Hirose, T., and Shinoda, K. (2005). Raman Spectra od Normal Modes and Disorder in Monoclinic tridymite and its Higher Temperature Orthorhombic Modification. *Journal of Mineralogical and Petrological Sciences*. **100**: 91-103.

Lane, M. (2007). Mid-Infrared Emission Spectroscopy of Sulfate and Sulfate-Bearing Minerals. *American Mineralogist*. **92**:1-18.

Larkin, P. (2011). Infrared and Raman Spectroscopy: Principles and Spectral Interpretation. *Elsiever.*

Mouri, T. and Enami, M. (2008). Raman Spectroscopic Study of Olivine-Group Minerals. *Journal of Mineralogical and Petrological Sciences*. **103**:100-104.

Nelson, J.(2014). Mars Exploration Rovers. *NASA*. Retrieved on February 26, 2021.

Nestola, F., Mittempergher, S., Di Toro, G., Zorzi, FD., and Pedron, D. (2010). Evidence of Dmisteinbergite in Pseudotachylyte: A Tool to Constrain the Thermal History of a Seismic Event. *American Mineralogist*. **95**:405–409.

Pelletier, M. (2003). Quantitative Analysis Using Raman Spectrometry. *Focal point.* **57**(1):21.

Piriou, B. and McMillan, P. (1993). The High-Frequency Vibrational Spectra of Vitreous and Crystalline Orthosilicates. *American Mineralogist*. **68**:426-443.

Popescu, M. (2012). Techniques for asteroid spectrocopy. Paris: *HAL*.

Robin, J., David, H., Liwu, Z., Daniel, W., & Ventsislav, V. (2019). Raman Techniques: Fundamentals and Frontiers. *Springer Open*.

Smith, B. (2019). A Guide to Reading Raman Spectra. *AZO Materials*.

Tarcea, N., Frosch, T., Rösch, P., Hilchenbach, M., Stuffler, T., Hofer, S., *et al.* (2007). Raman Spectroscopy: A Powerful Tool for *in situ* Planetary Science. München: *Springer Science+Business Media B.V.*

Taylor, A. (2020). Photos: NASA Prepares to Launch the Mars Rover Perseverance. *The Atlantic.*

Wang, A., Jolliff, B., and Haskin, L. (1995). Raman Spectroscopy as a Method for Mineral Identification on Lunar Robotic Exploration Missions. *Journal of Geophysical Research*. **100**(l0):2.

Wilcock, L. (2021). Raman Spectra Explained. Renishaw plc.

Yoshimitsu, T.; Sasaki, S.; Yanagisawa, M.; Kubota, T. (2010). Scientific capability of Minerva rover in Hayabusa asteroid mission. *Lunar and Planetary Science*. **35**: 1517–1518.

Zhao, K. and Bai, F. (2020). Crystallinity and Play-of-Color in Gem Opal with Digit Patterns from Wegel Tena, Ethiopia. Minerals. **10**(625):8-9.

Appendix

The data files of minerals used to support this study can be found on http://rruff.info/. Further specific details in the data and results shall be delivered by the corresponding author upon request.

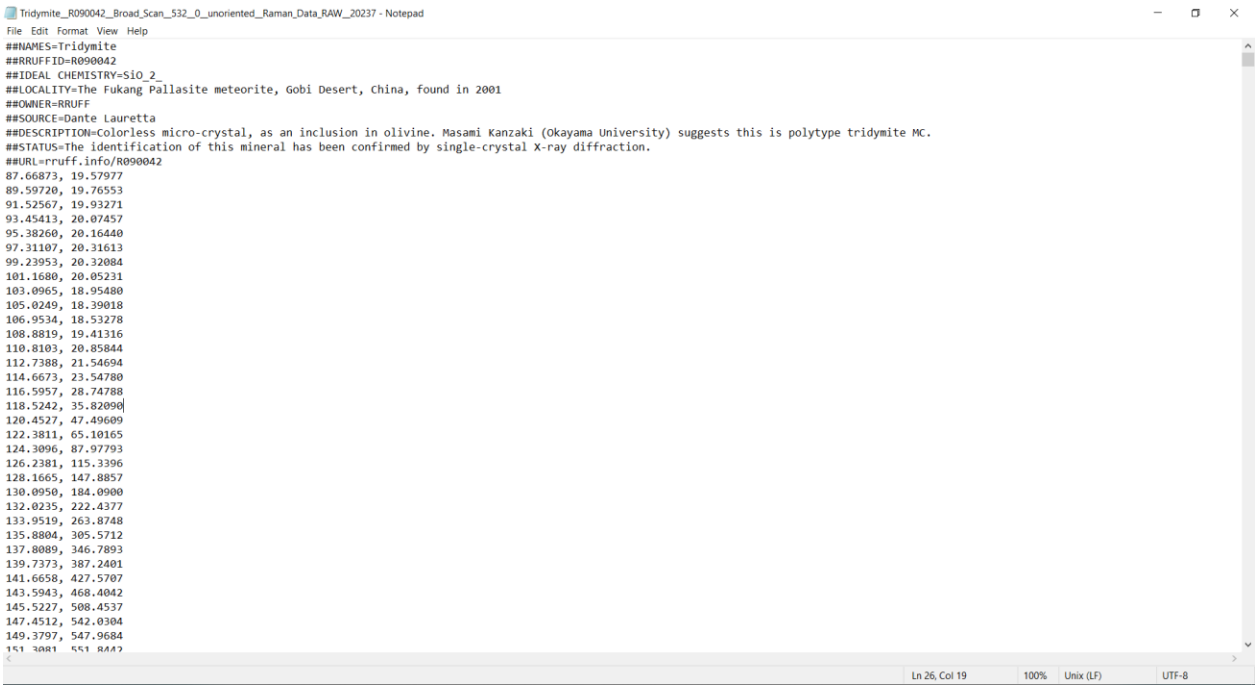

Figure 33: Raman Data of Tridymite from the Fukang Pallasite Meteorite. (Source: rruff.info/)

Figure 34: Raman Data of Tridymite from the Mount Howe 88403 Meteorite. (Source: rruff.info/)

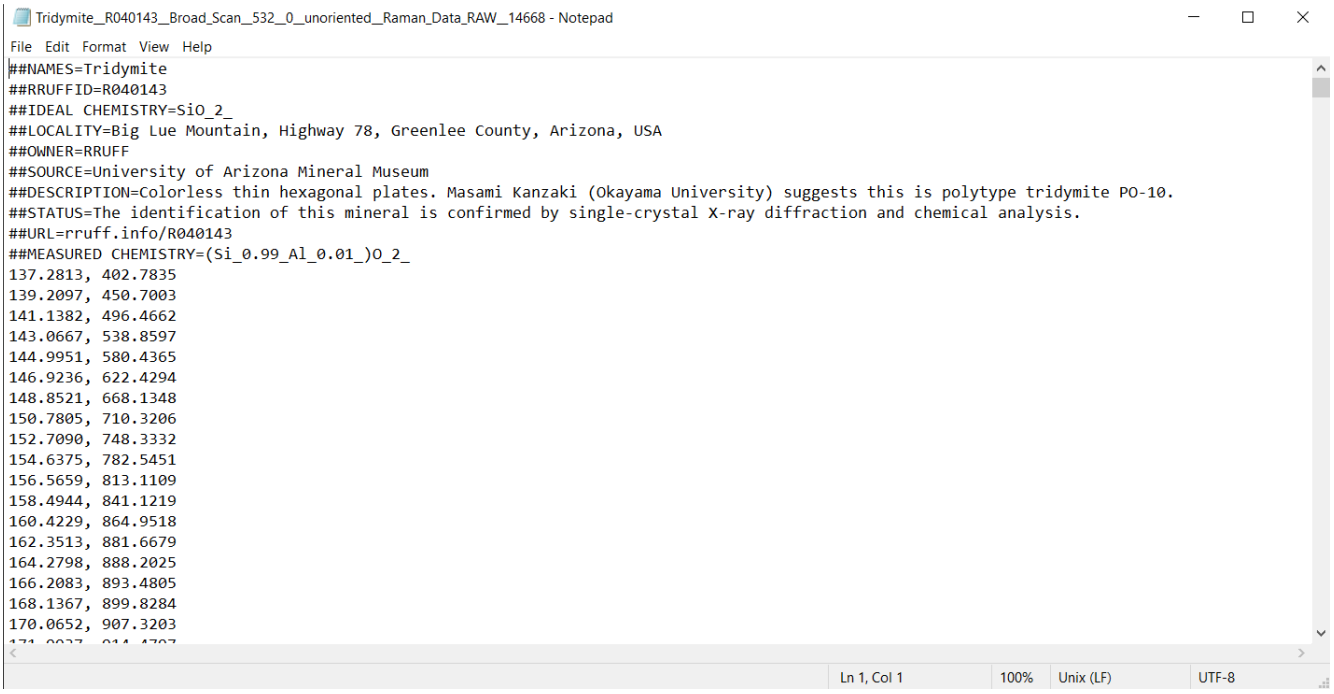

Figure 35: Raman Data of Tridymite from Big Lue Mountain, an Earthly Origin. (Source: rruff.info/)

Figure 36: Raman Data of a Synthetic Tridymite. (Source: rruff.info/)

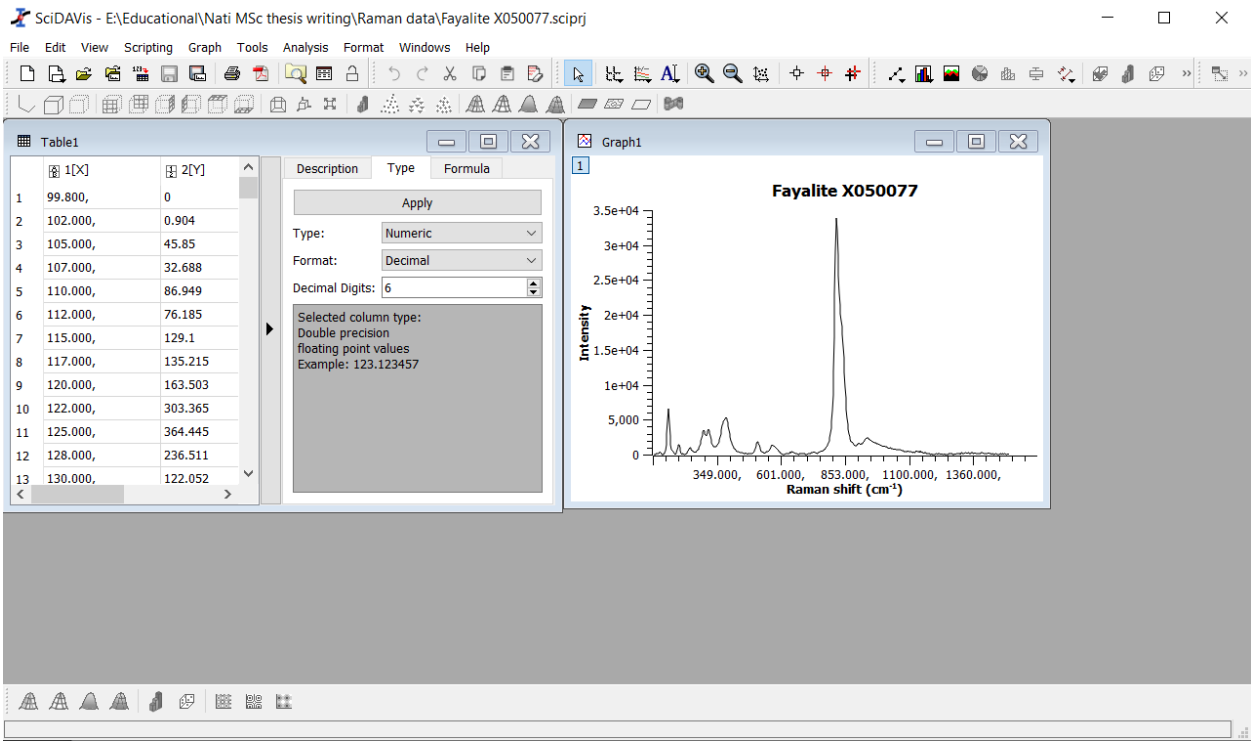

Figure 37: Graphical illustration of Raman data by SciDAVis.